The Astrophysical Journal, 817:112 (19pp), 2016 February 1 doi:10.3847/0004-637X/817/2/112

A PROPER MOTION SURVEY USING THE FIRST SKY PASS OF *NEOWISE*-REACTIVATION DATA

Adam C. Schneider[1], Jennifer Greco[1], Michael C. Cushing[1], J. Davy Kirkpatrick[2], Amy Mainzer[3], Christopher R. Gelino[2,4], Sergio B. Fajardo-Acosta[2], and James Bauer[3]
[1] Department of Physics and Astronomy, University of Toledo, 2801 W. Bancroft St., Toledo, OH 43606, USA; Adam.Schneider@Utoledo.edu
[2] Infrared Processing and Analysis Center, MS 100-22, California Institute of Technology, Pasadena, CA 91125, USA
[3] Jet Propulsion Laboratory, California Institute of Technology, Pasadena, CA 91125, USA
[4] NASA Exoplanet Science Institute, Mail Code 100-22, California Institute of Technology, 770 South Wilson Ave, Pasadena, CA 91125, USA
Received 2015 October 2; accepted 2015 November 30; published 2016 January 26

ABSTRACT

The *Wide-field Infrared Survey Explorer* (*WISE*) was reactivated in 2013 December (*NEOWISE*) to search for potentially hazardous near-Earth objects. We have conducted a survey using the first sky pass of *NEOWISE* data and the AllWISE catalog to identify nearby stars and brown dwarfs with large proper motions ($\mu_{\rm total} \gtrsim 250$ mas yr^{-1}). A total of 20,548 high proper motion objects were identified, 1006 of which are new discoveries. This survey has uncovered a significantly larger sample of fainter objects ($W2 \gtrsim 13$ mag) than the previous *WISE* motion surveys of Luhman and Kirkpatrick et al. Many of these objects are predicted to be new L and T dwarfs based on near- and mid-infrared colors. Using estimated spectral types along with distance estimates, we have identified several objects that likely belong to the nearby solar neighborhood ($d < 25$ pc). We have followed up 19 of these new discoveries with near-infrared or optical spectroscopy, focusing on potentially nearby objects, objects with the latest predicted spectral types, and potential late-type subdwarfs. This subset includes six M dwarfs, five of which are likely subdwarfs, as well as eight L dwarfs and five T dwarfs, many of which have blue near-infrared colors. As an additional supplement, we provide 2MASS and AllWISE positions and photometry for every object found in our search, as well as 2MASS/AllWISE calculated proper motions.

Key words: brown dwarfs – stars: low-mass

Supporting material: machine-readable tables

1. INTRODUCTION

Nearby stars and brown dwarfs serve as benchmarks for many vital areas of astrophysics, both as individual objects and as an ensemble. As individual objects, they are particularly attractive as astrophysical laboratories because they are the brightest examples of their spectral type, and are therefore optimal targets for detailed studies of a given class. Nearby brown dwarfs also provide the best examples with which to study cold, exoplanet-like atmospheres across a variety of physical parameters (e.g., surface gravity, metallicity), thus offering critical checks of theory. As a population, nearby low-mass objects probe the efficiency (or lack thereof) of star formation at low masses, and as a result provide detailed information on the shape and cutoff of the initial mass function in a regime (<30 Jupiter masses) that is difficult to study in sites of active star formation (e.g., Kirkpatrick et al. 2012). Cataloguing the nearest solar neighbors, however, is not a straightforward procedure. Indeed, recent discoveries have demonstrated that some of our closest neighbors have been lurking unseen because of their low temperatures and luminosities (e.g., WISE J052126.29+102528.4 (~5 pc), Bihain et al. 2013; WISE J104915.57–531906.1AB (~2 pc), Luhman 2013; WISEA J154045.67–510139.3 (~5.9 pc), Kirkpatrick et al. 2014; WISE J085510.83–071442.5 (~2 pc), Luhman 2014b; and WISE J072003.20–084651.2 (~7 pc), Scholz 2014).

Most searches for nearby very-low-mass stars and brown dwarfs have used red optical through mid-infrared colors as the main selection criterion due to the shift in the peak wavelength of the Planck function with decreasing effective temperature (e.g., Kirkpatrick et al. 1999, 2011; Leggett et al. 2000). While such searches are geared toward finding objects with normal gravities and solar-like metallicities, they are generally biased against uncovering objects with unusual characteristics. Kinematic searches, on the other hand, avoid such a bias by using proper motion alone as a judge of distance. By identifying objects with large proper motions, unusual brown dwarfs overlooked by previous surveys can be identified (e.g., Metchev et al. 2008; Deacon et al. 2009; Sheppard & Cushing 2009; Artigau et al. 2010; Kirkpatrick et al. 2010; Deacon et al. 2011; Gizis et al. 2011; Liu et al. 2011; Scholz et al. 2011, 2012; Scholz 2014).

Multi-epoch data from the *Wide-field Infrared Survey Explorer* (*WISE*) have enabled the first all-sky motion searches using solely mid-infrared wavelengths, which allows for the straightforward identification of low-mass stars and brown dwarfs in a wavelength region where they emit their peak flux. The motion survey of Luhman (2014a) and the AllWISE motion survey (Kirkpatrick et al. 2014) used data from the primary *WISE* mission to uncover thousands of new objects with significant proper motions, including the aforementioned WISE J104915.57–531906.1AB, WISE J085510.83–071442.5, and WISEA J154045.67–510139.3, along with a wealth of previously unknown late-type subdwarfs (Kirkpatrick et al. 2014; Luhman & Sheppard 2014). Most of these discoveries were identified using a six-month time baseline between *WISE* epochs (~20% of the sky was covered with an additional third epoch, resulting in a time baseline of one year). Despite the successes of the Luhman and Kirkpatrick et al. studies, each survey missed objects that the other one found, due to their different candidate selection procedures, suggesting that there are likely more nearby objects to be discovered. Of the 3525 and 762 discoveries in Kirkpatrick et al. (2014) and

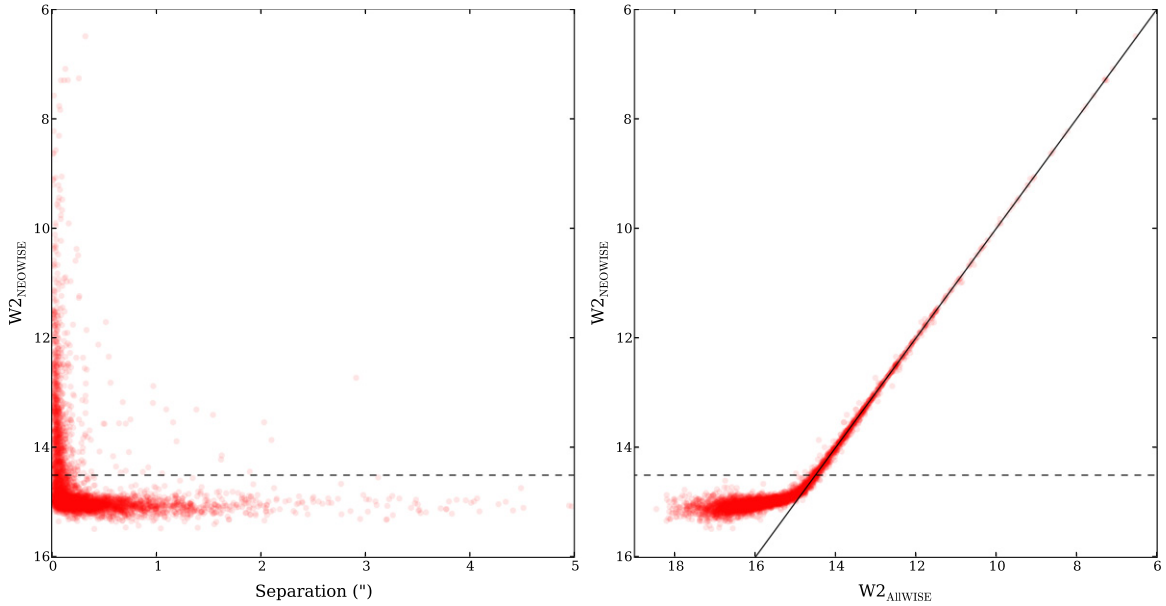

Figure 1. Left: the *NEOWISE W2* magnitude as a function of separation between the AllWISE and *NEOWISE* source catalog positions for a random sample of 5000 objects. The dashed line indicates a *NEOWISE W2* magnitude of 14.5. Right: a comparison of the *NEOWISE W2* and AllWISE *W2* magnitudes. The solid line indicates a ratio of unity. The dashed line indicates a *NEOWISE W2* magnitude of 14.5.

Luhman (2014a), respectively, only 321 were common to both surveys.

WISE was reactivated in 2013 December to search for potentially hazardous near-Earth objects (*NEOWISE*; Mainzer et al. 2014). We have completed a survey whereby we used the individual detections from the first *NEOWISE* pass of the sky in combination with the AllWISE source catalog to identify previously overlooked stars and brown dwarfs with large proper motions. Our goals are to (1) identify late-type subdwarf candidates to further map the existence and extent of the putative subdwarf gap (Kirkpatrick et al. 2014) in order to place constraints on brown dwarf cooling theory, (2) identify overlooked nearby stars and brown dwarfs, which can have a significant impact on investigations of the initial mass function of the local population, and (3) identify brown dwarfs with unusual characteristics (e.g., binaries). In Section 2, we describe the search strategy for the *NEOWISE* proper motion survey, while the results are presented in Section 3. In Sections 4 and 5 we describe the follow-up spectroscopic observations and an analysis of a subset of discoveries from this effort.

2. IDENTIFYING OBJECTS WITH HIGH PROPER MOTIONS

The *NEOWISE* reactivation mission was carried out using the *W1* (3.4 μm) and *W2* (4.6 μm) passbands of the *WISE* telescope. Because the intent of the *NEOWISE* observations is the identification of near-Earth objects, the images are not co-added like the previous epochs of *WISE* data. However, the detections from each individual *WISE* frame are collected into a single catalog. Since the *NEOWISE* images are not co-added, the first step in identifying high proper motion objects is to construct a source catalog from the *NEOWISE* Single Exposure Source Table.

One of the principal goals of our *NEOWISE* proper motion survey is to search for cold, nearby brown dwarfs. Since such objects are typically too faint to be detected in *W1*, we conducted our search using *W2* data. For the additional science goals (i.e., identifying nearby M and L-type subdwarfs), the difference between *W1* and *W2* is small (*W1*–*W2* values for late-type subdwarfs in Table 6 of Kirkpatrick et al. (2014) range from 0.10 to 0.56 mag), so a search in *W2* alone will be sufficient to identify most objects of interest. Our *NEOWISE* source table is assembled using the individual detections of each source with the aid of the STILTS tool set (Taylor 2006), a method very similar to that used in Luhman (2014a). STILTS is a set of command line tools designed specifically to handle large tables. Sources in our *NEOWISE* source catalog are required to have at least five single detections within a 1.″5 radius, where the individual *W2* magnitudes of each detection are off by no more than one magnitude from the median of all the other individual detections. We consider all detections that occur within 10 days to form a single epoch. A length of 10 days was chosen to account for the *WISE* telescope's moon avoidance maneuvers. We also require the individual detections to not be flagged as artifacts (i.e., *cc_flags* ≠ ["D," "H," "O," "P"]). Lastly, we avoid the ecliptic poles (abs(elat) ⩽ 85.°0) because the depth of coverage at the poles creates an extremely large amount of data for a relatively small area of the sky. The final product of this process is a *NEOWISE* source catalog consisting of average right ascension, declination, *W1*, *W2*, and modified Julian Date values for each source.

The accuracy of the astrometric and photometric measurements of sources in our *NEOWISE* source catalog decreases as objects become fainter in *W2*. To identify the practical limits of our *W2* magnitude search, we cross-matched a random sample of 5000 entries from our *NEOWISE* source catalog (which should largely be unmoving background sources) with the AllWISE source catalog using a 5″ search radius. The separation between the AllWISE and *NEOWISE* source positions as a function of the *NEOWISE W2* magnitude, as well as a comparison between the *NEOWISE* and AllWISE *W2* magnitudes, is shown in Figure 1. The figure shows that below a *NEOWISE W2* magnitude of ∼14.5, the positional and

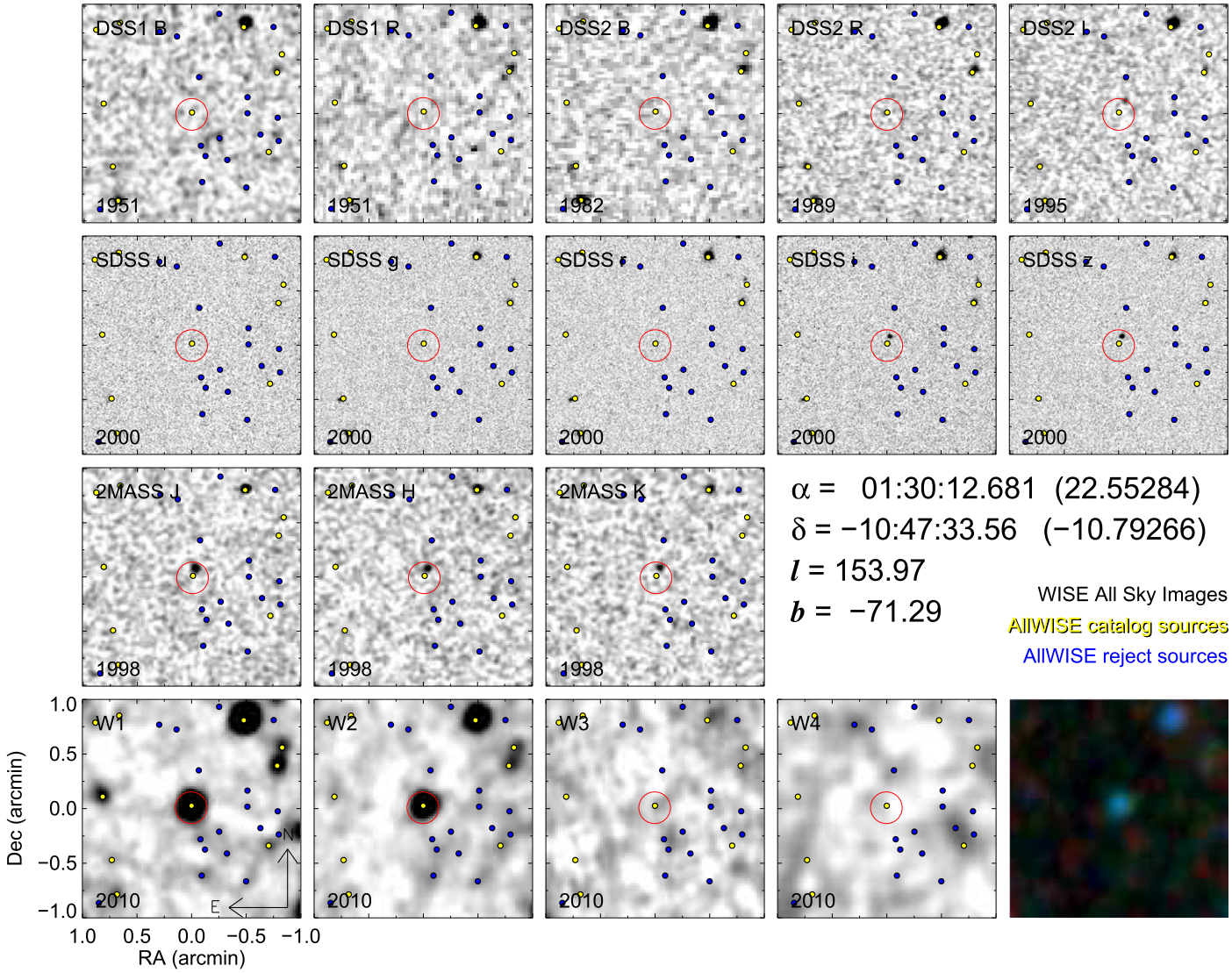

Figure 2. Optical (DSS1, DSS2, SDSS), near-infrared (2MASS), and mid-infrared (*WISE* All-sky) images of the newly discovered high proper motion object WISEA J013012.66–104732.4. The red circle indicates the *NEOWISE* position of WISEA J013012.66–104732.4. Yellow points indicate the positions of sources in the AllWISE source catalog, while blue points indicate the positions of sources in the AllWISE reject catalog.

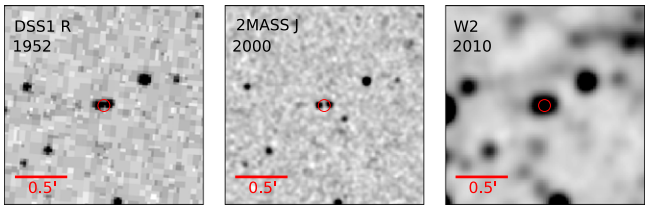

Figure 3. 2MASS and AllWISE images of a high proper motion candidate determined to be spurious. The red circle denotes the *NEOWISE* position of the candidate.

photometric *NEOWISE* values become unreliable. We therefore make a $W2 \leqslant 14.5$ magnitude cut to our final source catalog for our initial input sample.

A typical proper motion survey will attempt to identify multiple detections of single objects at different epochs. Our search strategy differs in that we identify high proper motion candidates as those that do not have a match at the previous epoch within a small search radius. We identify potential high proper motion objects by cross-matching the positions of sources within our *NEOWISE* source catalog with the AllWISE catalog using a 1″ search radius, where those sources without matches are retained as potential high proper motion candidates. In addition, each source is cross-matched with the AllWISE reject catalog and the 2MASS point source catalog using a 1″ search radius, again retaining only those without a match. Cross-matching with the AllWISE reject catalog was necessary because we found that there are some instances where real objects near extremely bright sources can be flagged as artifacts, ending up in the AllWISE reject catalog instead of the AllWISE source catalog. In addition, we also found instances where there are real sources, usually blended with a slightly brighter source in the *WISE* images, that are in neither the AllWISE source or reject catalogs. These sources are typically resolved in 2MASS and listed in the 2MASS point source catalog, hence the 2MASS 1″ search.

Considering the ∼4 year time baseline between the first sky pass of *NEOWISE* and the first *WISE* epochs, our 1″ search radius gives us a nominal minimum proper motion limit of ∼250 mas yr^{-1}. We note that this limit is self-imposed, and that

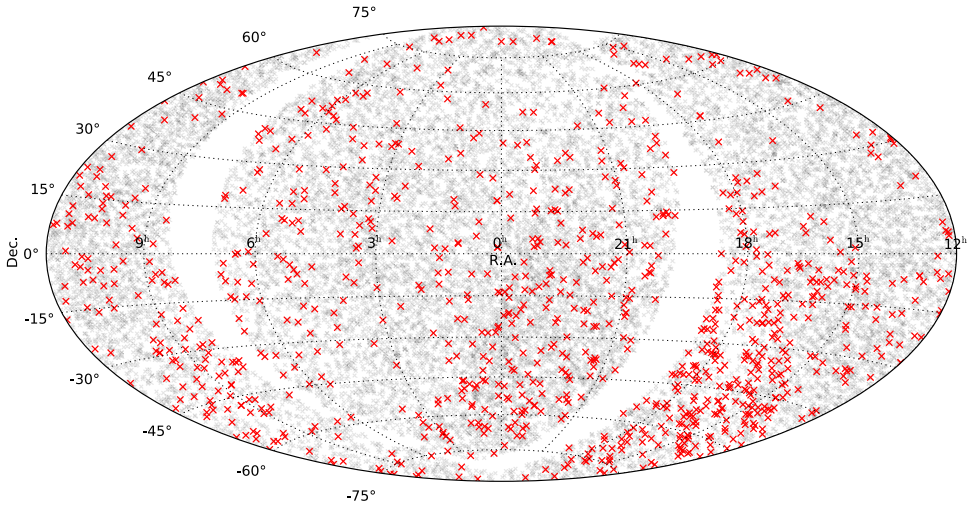

Figure 4. Equatorial positions of every high proper motion source found with our *NEOWISE* proper motion survey. Previously known objects with high proper motions are denoted by gray crosses, while new discoveries are plotted in red. The gaps in coverage are due to the *NEOWISE* command timing anomaly (see Section 3.1).

proper motions below this limit should also be detectable with the *NEOWISE*/AllWISE time baseline. By not requiring a significance of motion threshold as in Luhman (2014a), this survey probes to the faintest magnitude limits of what is possible with *WISE* single detections. Using this method, the only upper boundary for detecting proper motions is the size of the *WISE* images in our finder charts. Because the images are $2' \times 2'$, any object moving faster than $\sim 15'' \, \mathrm{yr}^{-1}$ ($1'/\sim 4$ year) would be beyond the boundary of the image. Note that the two highest proper motion objects known (Barnard's Star—$10\farcs4 \, \mathrm{yr}^{-1}$ (Barnard 1916) and WISE J085510.83–071442.5—$8\farcs1 \, \mathrm{yr}^{-1}$ (Luhman & Esplin 2014)) are both below this threshold and were recovered in our survey.

When a *NEOWISE* source was found to not have a counterpart within $1''$ in the AllWISE source catalog, the AllWISE reject catalog, or the 2MASS point source catalog, we created a finder chart by gathering available optical (DSS and SDSS), near-infrared (2MASS), and mid-infrared (*WISE* All-sky) images. Each individual finder chart was examined by eye in an attempt to confirm each candidate's high proper motion by inspecting images at previous epochs. A typical finder chart for a new high proper motion discovery is shown in Figure 2. Sources that were discarded as spurious were typically blended or extended in nature. Figure 3 shows an example of a high proper motion candidate that was determined to be a blended source (and therefore spurious) during the visual inspection process. Over one million proper motion candidates were scrutinized in this way.

3. DISCUSSION

3.1. Survey Results

A total of 20,548 high proper motion objects were found with the *NEOWISE* survey. In order to determine if a confirmed proper motion source is known or is a new discovery, we rely primarily on the SIMBAD database. We also checked catalogs of targeted searches for high proper motion objects (e.g., Pokorny et al. 2004; Lépine & Shara 2005; Deacon & Hambly 2007; Boyd et al. 2011; Luhman 2014a, and Kirkpatrick et al. 2014). Note that we only cross-match with catalogs made up of bona fide proper motion sources, not unvetted lists of candidates (e.g., Gagné et al. 2015). The vast majority of these objects were previously known to have significant proper motions. The number of new high proper motion discoveries from this search totaled 1006.

Figure 4 shows the locations of all high proper motion objects identified in our *NEOWISE* survey. The two gaps in coverage are due to a command timing anomaly that temporarily put the *NEOWISE* spacecraft in safe-mode (see the *NEOWISE* Data Release Explanatory Supplement for more details[5]). Similar to Kirkpatrick et al. (2014), most of the newly discovered high proper motion objects from this survey are located in the southern hemisphere, particularly near the Galactic center. This is because, historically, there have been more targeted high proper motion searches in the northern hemisphere and the Galactic center is an exceptionally confused area because of its high density of stars. We provide 2MASS and AllWISE associations, and 2MASS to AllWISE calculated proper motions for every newly discovered object in Table 1. Proper motion uncertainties come from the 2MASS and AllWISE positional uncertainties. The same information for every previously known high proper motion object is provided in Table 2. Upper limits for all magnitudes in all tables are at the 95% confidence level.[6]

Seven objects were found to be moving upon visual inspection of their finder charts, but did not have a corresponding entry in any of the *WISE* catalogs based on co-added images (AllWISE, All-sky, or Reject). All of these objects but one (WISEA 19501894+2530402) are blended with a nearby, brighter source, which likely led to their omission from the *WISE* catalogs. Three of these objects are new discoveries, while the other four are known high proper motion objects. 2MASS designations and photometry for all objects without *WISE* detections are provided in Table 3.

There were also a total of 51 confirmed high proper motion objects for which there were no 2MASS counterparts. Two of the objects are new discoveries, while the remainder are known

[5] http://wise2.ipac.caltech.edu/docs/release/*NEOWISE*/expsup/sec1_2.html

[6] http://wise2.ipac.caltech.edu/docs/release/allwise/expsup/sec2_1.html and http://www.ipac.caltech.edu/2mass/releases/allsky/doc/sec4_4d.html

Table 1
New High Proper Motion Objects

AllWISE Designation	*W1* (mag)	*W2* (mag)	2MASS Designation	2MASS J (mag)	2MASS H (mag)	2MASS K_S (mag)	μ_α (mas yr^{-1})	μ_δ (mas yr^{-1})	Type[e] (photometric)
J000021.36+822940.1	14.057 ± 0.026	13.737 ± 0.031	00002008+8229395	15.060 ± 0.043	14.617 ± 0.062	14.316 ± 0.077	253.0 ± 13.2	68.1 ± 8.0	6.2
J000211.43–135749.0	12.890 ± 0.025	12.676 ± 0.025	00021121–1357480	13.973 ± 0.027	13.492 ± 0.035	13.138 ± 0.033	265.9 ± 7.1	−79.0 ± 6.3	6.3
J000430.66–260402.3	15.211 ± 0.038	14.127 ± 0.044	00043065–2603596	16.487 ± 0.133	15.587 ± 0.129	>15.523	11.9 ± 15.3	−229.6 ± 13.8	20.5
J000458.47–133655.1[a]	15.120 ± 0.037	14.457 ± 0.056	⋯	16.841 ± 0.171	16.120 ± 0.207	>15.410	431.3 ± 21.8	−37.4 ± 20.3	16.9
J000502.05+021714.2	12.450 ± 0.023	12.228 ± 0.023	00050184+0217120	13.686 ± 0.029	13.056 ± 0.035	12.675 ± 0.023	328.1 ± 7.4	216.6 ± 7.3	6.8
J000534.07–475033.0	14.694 ± 0.030	14.412 ± 0.046	00053380–4750280	15.816 ± 0.077	15.129 ± 0.094	14.858 ± 0.118	248.3 ± 11.9	−460.8 ± 10.3	5.0
J000536.63–263311.8	14.924 ± 0.033	14.261 ± 0.047	00053630–2633123	17.171 ± 0.225	15.849 ± 0.165	15.191 ± 0.154	384.0 ± 22.8	39.8 ± 20.5	17.1
J000551.34+021616.0	13.580 ± 0.026	13.351 ± 0.031	00055109+0216145	14.614 ± 0.024	14.009 ± 0.049	13.699 ± 0.059	382.7 ± 9.5	141.2 ± 8.6	<5
J000603.34–522744.3	13.604 ± 0.026	13.340 ± 0.029	00060303–5227433	15.753 ± 0.070	14.794 ± 0.080	14.058 ± 0.061	282.4 ± 8.5	−97.7 ± 8.4	13.5
J000627.85+185728.8	14.111 ± 0.027	13.785 ± 0.039	00062779+1857320	17.138 ± 0.206	15.686 ± 0.152	14.836 ± 0.084	72.2 ± 15.7	−289.1 ± 14.8	16.1
J000856.39–281321.7	14.119 ± 0.027	13.636 ± 0.037	00085614–2813211	16.727 ± 0.137	15.664 ± 0.139	15.049 ± 0.131	284.3 ± 16.0	−54.7 ± 13.6	18.0
J001320.75+271020.4	14.538 ± 0.030	14.356 ± 0.047	00132036+2710222	15.500 ± 0.060	14.884 ± 0.069	14.729 ± 0.112	404.8 ± 7.5	−132.8 ± 7.5	<5
J001422.56–333734.8	13.889 ± 0.026	13.612 ± 0.034	00142232–3337332	14.886 ± 0.045	14.377 ± 0.054	14.076 ± 0.068	254.7 ± 7.5	−134.6 ± 7.5	<5
J001643.97+230426.5	14.325 ± 0.029	13.667 ± 0.035	00164364+2304262	>16.412	15.704 ± 0.138	>14.973	386.1 ± 16.7	25.9 ± 15.8	18.9
J002000.06–070950.5	13.747 ± 0.027	13.435 ± 0.033	00195978–0709505	14.754 ± 0.034	14.200 ± 0.044	13.849 ± 0.044	358.5 ± 11.8	−5.3 ± 11.8	<5

Notes.
[a] 2MASS photometry for this object is from the 2MASS Reject Catalog.
[b] *WISE* photometry and positions for this object are from the AllWISE Reject Catalog.
[c] *WISE* photometry and positions for this object are from the *WISE* All-sky Catalog.
[d] This object is a co-moving double that is resolved in 2MASS, but not in AllWISE.
[e] Numerical spectral type estimates (e.g., 5 = M5, 15 = L5, 25 = T5)

(This table is available in its entirety in machine-readable form.)

Table 2
Known High Proper Motion Objects

AllWISE Designation	*W1* (mag)	*W2* (mag)	2MASS Designation	2MASS J (mag)	2MASS H (mag)	2MASS K_S (mag)	μ_α (mas yr^{-1})	μ_δ (mas yr^{-1})
J000012.91–545452.7	10.383 ± 0.023	10.379 ± 0.021	00001260–5454517	10.722 ± 0.020	10.475 ± 0.025	10.449 ± 0.023	249.3 ± 7.3	−89.8 ± 6.5
J000027.09+575404.9	11.734 ± 0.023	11.733 ± 0.023	00002657+5754025	12.497 ± 0.024	12.010 ± 0.031	11.855 ± 0.028	381.1 ± 6.7	219.1 ± 6.7
J000028.04–412531.3	12.685 ± 0.023	12.548 ± 0.024	00002754–4125310	13.545 ± 0.026	12.974 ± 0.022	12.834 ± 0.032	506.6 ± 7.4	−33.8 ± 6.6
J000031.00–261352.0	9.328 ± 0.023	9.286 ± 0.020	00003078–2613533	10.400 ± 0.029	9.753 ± 0.031	9.523 ± 0.024	298.2 ± 7.9	124.8 ± 7.8
J000031.98+650427.7	11.285 ± 0.023	11.144 ± 0.020	00003151+6504287	12.126 ± 0.022	11.558 ± 0.031	11.393 ± 0.021	274.3 ± 6.5	−86.0 ± 6.5
J000034.69–365006.8	10.809 ± 0.023	10.718 ± 0.020	00003429–3650079	11.698 ± 0.022	11.095 ± 0.023	10.912 ± 0.023	428.0 ± 7.3	105.7 ± 7.2
J000037.66+420712.8	11.682 ± 0.024	11.614 ± 0.021	00003735+4207123	12.581 ± 0.022	11.958 ± 0.024	11.800 ± 0.024	300.2 ± 6.9	49.1 ± 6.1
J000039.50+182921.9	7.506 ± 0.033	7.556 ± 0.020	00003925+1829198	8.443 ± 0.019	7.794 ± 0.023	7.639 ± 0.018	324.0 ± 8.8	193.9 ± 6.2
J000040.37+162804.4	12.985 ± 0.024	12.738 ± 0.026	00004004+1628047	14.061 ± 0.031	13.519 ± 0.041	13.159 ± 0.037	441.2 ± 7.7	−27.8 ± 6.8
J000040.56+031339.3	12.849 ± 0.024	12.618 ± 0.026	00004044+0313424	13.711 ± 0.026	13.212 ± 0.031	12.964 ± 0.030	167.5 ± 12.7	−307.3 ± 8.2
J000044.53–502924.7	10.387 ± 0.023	10.230 ± 0.020	00004412–5029248	11.215 ± 0.030	10.726 ± 0.026	10.486 ± 0.024	394.2 ± 7.9	6.3 ± 7.0
J000045.68–624345.6	8.992 ± 0.023	9.042 ± 0.020	00004539–6243437	9.885 ± 0.023	9.230 ± 0.023	9.070 ± 0.023	204.5 ± 6.9	−186.0 ± 6.9
J000047.16–351007.1	8.109 ± 0.022	8.072 ± 0.021	00004688–3510060	9.117 ± 0.029	8.480 ± 0.040	8.282 ± 0.027	343.2 ± 7.7	−111.5 ± 6.8
J000047.26–054116.7	12.797 ± 0.023	12.631 ± 0.027	00004707–0541187	13.789 ± 0.024	13.196 ± 0.022	12.927 ± 0.027	257.3 ± 12.5	184.0 ± 6.8
J000052.23+143402.2	9.057 ± 0.024	9.009 ± 0.020	00005198+1434028	10.014 ± 0.019	9.382 ± 0.028	9.155 ± 0.023	345.4 ± 10.7	−60.1 ± 7.2

Notes.
[a] 2MASS photometry for this object is from the 2MASS Reject Catalog.
[b] *WISE* photometry and positions for this object are from the AllWISE Reject Catalog.
[c] *WISE* photometry and positions for this object are from the *WISE* All-sky Catalog.
[d] This object is a co-moving double that is resolved in 2MASS, but not in AllWISE.

(This table is available in its entirety in machine-readable form.)

Table 3
Objects Lacking an Entry in the *WISE* All-sky and AllWISE Source Catalogs and Reject Tables

2MASS Designation	2MASS J (mag)	2MASS H (mag)	2MASS K_S (mag)
Known High Proper Motion Objects			
01570561–5925475	11.695 ± 0.027	11.076 ± 0.027	10.777 ± 0.025
19501894+2530402	14.246 ± 0.027	13.648 ± 0.031	13.468 ± 0.045
21225632+3656001	13.712 ± 0.031	13.304 ± 0.036	13.117 ± 0.030
23164596–4047396	13.944 ± 0.026	13.447 ± 0.022	13.213 ± 0.034
New Discoveries			
16161420–6146542	14.597 ± 0.035	14.138 ± 0.045	13.855 ± 0.054
16350859–3832440	13.168 ± 0.026	12.642 ± 0.032	12.343 ± 0.033
16411478–3215156	14.034 ± 0.028	13.403 ± 0.033	13.276 ± 0.038

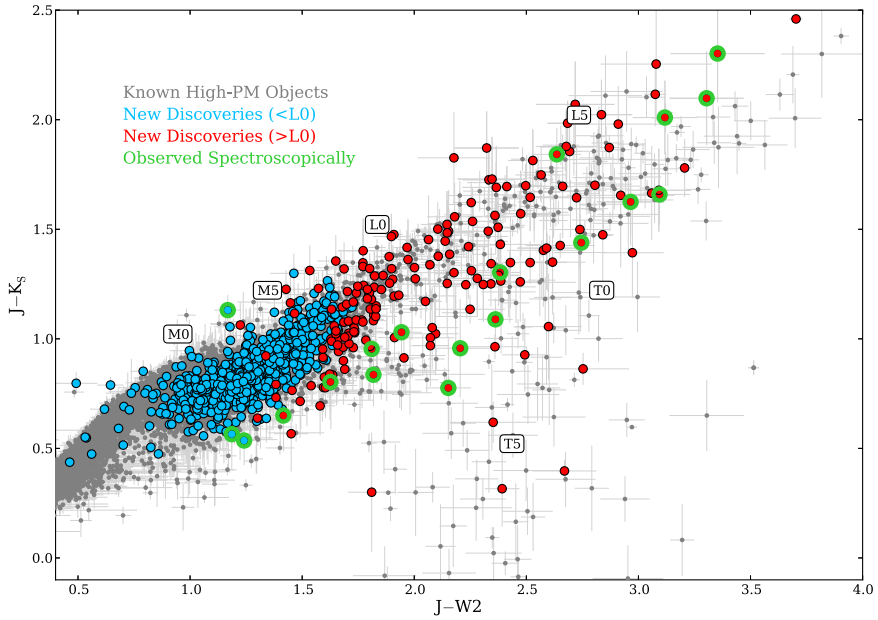

Figure 5. $J - K_S$ vs. $J - W2$ color–color diagram for all high proper motion objects found with the *NEOWISE* survey. Gray symbols are known objects from Table 2. Light blue circles are new discoveries with spectral type estimates earlier than L0. All other new discoveries are in red. Objects that have been followed up spectroscopically are highlighted in green. The approximate locations of M0, M5, L0, L5, T0, and T5 spectral types in this color space are labeled for reference. Objects without 2MASS counterparts are not included in this figure.

T and Y dwarfs. These two new discoveries are further discussed in Section 3.4. AllWISE designations and photometry for all high proper motion objects without 2MASS detections are provided in Table 4.

3.2. Categorizing Discoveries

In order to identify the most interesting objects for follow-up spectroscopic observations (e.g., nearby objects and late-type subdwarfs), we attempted to estimate the approximate spectral type of each new discovery using the available 2MASS and AllWISE photometry. This was accomplished by using the k-Nearest Neighbors (k-NN) classification scheme described in the Appendix. The last column of Table 1 gives the estimated numerical type for each new discovery (e.g., 5 = M5, 15 = L5, 25 = T5). We chose to list numerical types to ensure that these estimates are not mistaken for actual spectral types determined from optical or near-infrared spectroscopy. Note that the earliest estimated types from our classification scheme are M0, so any object with an earlier spectral type than M0 will likely be classified as early M using this method. However, as we are most interested in late-type dwarfs (spectral types L and T), this does not affect our follow-up target prioritization. For this reason, we only provide final photometric types for objects with estimated types later than M5. Uncertainties for these types are typically ∼2 subtypes (see the Appendix).

Figure 5 shows the $J - K_S$ versus $J - W2$ color–color diagram for all high proper motion objects found during this survey. The large cluster of sources at $J - K_S \sim 0.7$ and $J - W2 \sim 1.3$ are early to mid-M dwarfs, which make up the vast majority of our new discoveries. Several new discoveries at the edges of the main M dwarf clump are classified as having types later than L0, which may show that our technique of estimating spectral types photometrically may have difficulty properly classifying color outliers.

3.3. Common Proper Motion Pairs

During the vetting process of confirming high proper motion candidates, several new objects were noted to possibly be co-moving with a known high proper motion star. Note that we did not perform a specific search for common proper motion pairs; we have only noted those that were noticed during the proper motion verification process of this survey. Therefore, this list of common proper motion pairs is likely not exhaustive. All potential new pairs are listed in Table 5, along with their 2MASS to AllWISE proper motions.

Following Luhman & Sheppard (2014), we evaluate each pair using the companionship criterion proposed by Lépine & Bongiorno (2007), which all pairs pass. Table 6 provides additional information from the literature for the known high proper motion component of each pair. For those that have a parallax measurement, we also include the projected separation between the pair in AU. In each case, the *NEOWISE* discovery is the fainter component of the pair in *W1* and *W2* magnitude, with three exceptions. WISEA J184259.14–110921.6 is a companion to the white dwarf GJ 2139, which was not detected in the AllWISE catalog. WISEA J232308.63–631405.8 is slightly brighter in *W1* and *W2* than its known companion 2MASS J23230415–6314327. Lastly, WISEA J203126.63–333515.9 and its companion WISEA J203126.61–333504.2 are both new discoveries from this survey.

3.4. Nearby Objects

Using our estimated spectral types (with a ± 2 subtype uncertainty), *W2* magnitudes, and the absolute magnitude–spectral type relation for *W2* from Dupuy & Liu (2012), we estimate a distance range to every new discovery with an estimated spectral type later than M5 in an attempt to identify new nearby objects. We use the *W2* magnitude because each object in our new discovery list is detected with AllWISE (with the exception of the three new objects in Table 3) and has a *W2* magnitude $\lesssim$14.5, which corresponds to a signal-to-noise ratio (S/N) of ~15. We initially identified ~70 objects with distance estimates $\leqslant$25 pc. However, upon visual inspection of the finder charts, several high proper motion objects were found to be unresolved blends in the *WISE* images, which likely affected their photometry and led to erroneous spectral types. We visually inspected the finder charts for each of the ~70 objects potentially within 25 pc, flagging those that were blended in the *WISE* images. All of these blends contain a high proper motion source and an unrelated, stationary background source (i.e., none are co-moving doubles). Such blends can cause objects to be misclassified using our classification scheme, and will cause them to appear overluminous, and hence closer than they actually are. We omit all such blends from our list of potentially nearby sources. The remaining 46 objects are listed in Table 7. One object (WISEA J105515.71–735611.3) is estimated to be within ~10 pc, with a photometric type estimate of 7.4 (~M7). Three of these objects (WISEA J001643.97+230426.5, WISEA J003338.45+282732.4, and WISEA J010202.11+035541.4) have been followed up spectroscopically and are discussed further in Section 5.2.

In addition, there are two objects from our discovery list that have no 2MASS counterpart (see Section 3.1 and Table 4). Both of these discoveries (WISEA J030919.70–501614.2 and WISEA J133300.03–160754.4) have very red *W1* − *W2* colors (2.83 and 2.76, respectively), indicating spectral types $\geqslant$T7 for both objects (Kirkpatrick et al. 2012). Distance estimates for these two new late T dwarfs are 9–13 and 17–24 pc, respectively, for WISEA J030919.70–501614.2 and WISEA

Table 4
Objects Lacking 2MASS Counterparts

AllWISE Designation	*W1* (mag)	*W2* (mag)
Known High Proper Motion Objects		
J000517.49+373720.4	16.764 ± 0.089	13.291 ± 0.031
J001505.88–461517.8	16.960 ± 0.101	14.218 ± 0.043
J005911.10–011401.1	16.899 ± 0.118	13.732 ± 0.039
J033605.04–014351.0	18.449 ± 0.470	14.557 ± 0.057
J045853.91+643452.6	16.439 ± 0.074	13.022 ± 0.027
J061213.88–303612.1	16.402 ± 0.061	14.038 ± 0.038
J062309.92–045624.5	16.845 ± 0.094	13.814 ± 0.035
J074457.24+562820.9	17.181 ± 0.118	14.531 ± 0.049
J075946.98–490454.0	16.997 ± 0.091	13.812 ± 0.032
J085510.74–071442.5	16.231 ± 0.064	13.704 ± 0.033
J090116.20–030636.0	17.188 ± 0.129	14.557 ± 0.054
J092906.76+040957.6	16.543 ± 0.083	14.254 ± 0.048
J094306.00+360723.3	18.176 ± 0.297	14.413 ± 0.048
J095047.31+011733.1	17.635 ± 0.182	14.507 ± 0.051
J101243.44+102059.8	16.319 ± 0.073	14.180 ± 0.047
J102557.67+030755.8	17.487 ± 0.194	14.136 ± 0.052
J102940.51+093514.1	16.780 ± 0.117	14.376 ± 0.074
J105257.95–194250.1	16.585 ± 0.084	14.111 ± 0.044
J111239.25–385700.5	17.478 ± 0.169	14.404 ± 0.048
J115013.85+630241.3	16.958 ± 0.089	13.405 ± 0.028
J115239.94+113406.9	16.825 ± 0.106	14.649 ± 0.063
J120444.60–015034.7	16.573 ± 0.088	14.672 ± 0.060
J121710.27–031112.1	15.267 ± 0.039	13.205 ± 0.034
J121756.92+162640.3	16.549 ± 0.082	13.128 ± 0.030
J125715.91+400854.2	16.672 ± 0.079	14.431 ± 0.045
J131106.21+012253.9	17.579 ± 0.198	14.703 ± 0.060
J131833.96–175826.3	17.513 ± 0.160	14.666 ± 0.058
J132233.63–234017.0	16.733 ± 0.087	13.960 ± 0.040
J140518.32+553421.3	18.765 ± 0.396	14.097 ± 0.037
J145715.01+581510.1	16.661 ± 0.059	14.417 ± 0.037
J150115.92–400418.2	16.091 ± 0.060	14.233 ± 0.043
J150411.81+102715.4	16.215 ± 0.055	14.063 ± 0.039
J151906.63+700931.3	17.084 ± 0.069	14.138 ± 0.031
J154151.65–225024.9[a]	16.736 ± 0.165	14.246 ± 0.063
J161215.92–342028.5	17.415 ± 0.199	13.984 ± 0.045
J161441.47+173935.4	18.174 ± 0.266	14.226 ± 0.040
J165311.03+444422.7	16.485 ± 0.048	13.824 ± 0.029
J181210.83+272144.2	17.468 ± 0.143	14.196 ± 0.039
J182831.08+265037.6	>18.248	14.353 ± 0.045
J184124.74+700038.2	16.436 ± 0.044	14.355 ± 0.033
J201404.11+042409.0	17.296 ± 0.168	14.956 ± 0.069
J201920.75–114807.5	17.256 ± 0.152	14.305 ± 0.052
J205628.88+145953.6	16.480 ± 0.075	13.839 ± 0.037
J210200.14–442919.9	16.951 ± 0.111	14.139 ± 0.043
J215918.90+030502.4	14.887 ± 0.034	14.278 ± 0.048
J220905.75+271143.6	>18.831	14.770 ± 0.055
J225540.75–311842.0	16.550 ± 0.079	14.161 ± 0.045
J232035.37+144830.1	16.588 ± 0.082	14.341 ± 0.057
J232519.55–410535.1	17.064 ± 0.114	14.108 ± 0.040
New Discoveries		
J030919.70–501614.2	16.465 ± 0.057	13.631 ± 0.031
J133300.03–160754.4	17.698 ± 0.194	14.943 ± 0.069

Note.
[a] *WISE* photometry and positions for WISE J154151.65–225024.9 are from the *WISE* All-sky Catalog.

Table 5
New Common Proper Motion Pairs

AllWISE Designation	μ_α (mas yr^{-1})	μ_δ (mas yr^{-1})	Known High-pm Star	μ_α (mas yr^{-1})	μ_δ (mas yr^{-1})	Separation (arcsec)
J003537.62–763750.7	201.6 ± 7.5	−37.9 ± 6.1	L 26–46	222.9 ± 7.2	−22.4 ± 5.8	19.1
J014242.26+084824.3	129.0 ± 10.3	−126.7 ± 8.6	NLTT 5699	138.7 ± 9.2	−161.2 ± 7.3	17.8
J040854.34–675105.0	216.9 ± 8.9	118.8 ± 7.4	2MASS J04083969–6750597	247.6 ± 7.5	189.7 ± 6.1	80.3
J050816.76–333021.9	−65.8 ± 7.5	−290.8 ± 6.7	LTT 2180	−61.3 ± 6.9	−288.4 ± 6.1	13.9
J063228.30+264347.3	218.7 ± 7.5	35.9 ± 7.7	G 103–38	250.4 ± 5.7	34.7 ± 5.5	25.6
J155017.09–862927.3[a]	−296.1 ± 19.8	−245.3 ± 10.2	LHS 5302	−334.6 ± 17.8	−267.6 ± 7.4	12.2
J155039.10–504255.2	243.8 ± 6.5	−73.3 ± 6.4	GJ 599.1	271.5 ± 6.2	−70.4 ± 6.1	276.4
J165906.03–784505.3	−158.2 ± 8.1	−186.7 ± 7.2	NLTT 43745	−188.1 ± 7.7	−287.5 ± 6.8	20.9
J170027.83–220737.8[a]	−68.1 ± 24.7	−514.5 ± 55.7	2MASS J17002798–2207454	−85.2 ± 6.4	−466.5 ± 6.3	13.0
J184259.14–110921.6	−208.4 ± 6.6	−271.2 ± 6.4	GJ 2139[b]	−246	−255	34.2
J191648.99+470032.2	−8.3 ± 7.2	282.3 ± 5.7	HD 181096	−19.1 ± 11.6	288.7 ± 10.2	40.6
J202422.29–063833.9	94.2 ± 8.7	−205.0 ± 7.9	2MASS J20242285–0638224	75.9 ± 8.1	−231.5 ± 7.1	12.9
J203126.63–333515.9[c]	112.9 ± 6.3	−138.6 ± 6.3	WISEA J203126.61–333504.2[c]	71.0 ± 6.1	−146.5 ± 5.9	12.5
J232308.63–631405.8	415.3 ± 8.3	23.5 ± 8.2	2MASS J23230415–6314327	417.9 ± 6.7	17.9 ± 6.6	37.1

Notes.
[a] The *WISE* designations for WISE J155017.09–862927.3 and WISE J170027.83–220737.8 are from the *WISE* All-sky catalog.
[b] For GJ 2139, we quote the proper motions reported in Stauffer et al. (2010), as this object is a white dwarf not detected in any *WISE* catalog.
[c] Both members of this pair are new discoveries.

Table 6
New Common Proper Motion Pair Properties

AllWISE Designation	Type[a] (photometric)	Known High-pm Star	Sp. Type	Ref.[b]	π (arcsec)	Ref.[b]	Fe/H	Ref.[b]	Separation (AU)
J003537.62–763750.7	7.2	L 26–46	⋯	⋯	11.06 ± 1.57	(4)	−0.15	(7)	1726
J014242.26+084824.3	7.1	NLTT 5699	⋯	⋯	⋯	⋯	⋯	⋯	⋯
J040854.34–675105.0	<5	2MASS J04083969–6750597	⋯	⋯	⋯	⋯	⋯	⋯	⋯
J050816.76–333021.9	6.8	LTT 2180	⋯	⋯	⋯	⋯	⋯	⋯	⋯
J063228.30+264347.3	10.7	G 103–38	K5	(1)	⋯	⋯	⋯	⋯	⋯
J155017.09–862927.3	<5	LHS 5302	⋯	⋯	⋯	⋯	⋯	⋯	⋯
J155039.10–504255.2[c]	<5	GJ 599.1	⋯	⋯	23.17 ± 1.84	(5)	−1.00	(7)	11929
J165906.03–784505.3	9.0	NLTT 43745	⋯	⋯	⋯	⋯	−1.32	(8)	⋯
J170027.83–220737.8[c]	7.1	2MASS J17002798–2207454	⋯	⋯	⋯	⋯	⋯	⋯	⋯
J184259.14–110921.6	<5	GJ 2139	DA4.9	(2)	53.0 ± 6.0	(6)	⋯	⋯	645
J191648.99+470032.2	<5	HD 181096	F6IV:	(3)	23.79 ± 0.32	(5)	−0.278	(9)	1706
J202422.29–063833.9	7.0	2MASS J20242285–0638224	⋯	⋯	⋯	⋯	⋯	⋯	⋯
J203126.63–333515.9	6.7	WISEA J203126.61–333504.2	⋯	⋯	⋯	⋯	⋯	⋯	⋯
J232308.63–631405.8	7.2	2MASS J23230415–6314327	⋯	⋯	⋯	⋯	⋯	⋯	⋯

Notes.
[a] Numerical spectral type estimates (e.g., 5 = M5, 15 = L5, 25 = T5).
[b] References: (1) Lee (1984), (2) Gianninas et al. (2011), (3) Hoffleit & Jaschek (1991), (4) Kordopatis et al. (2013), (5) van Leeuwen (2007), (6) Gliese & Jahreiß (1991), (7) Ammons et al. (2006), (8) Ryan et al. (1991), (9) Taylor (2005).
[c] The *WISE* designation for WISE J155017.09–862927.3 and WISE J170027.83–220737.8 are from the *WISE* All-sky catalog.

J133300.03–160754.4 based on spectral type estimates of T7 to T9. These objects are also listed in Table 7.

3.5. Late-type Subdwarfs

Subdwarfs are low-metallicity objects that are typically associated with the halo population, often having significantly larger tangential velocity ($V_{\rm tan}$) values than the field population. We select candidate late-type subdwarfs using two different strategies. First, as noted in Kirkpatrick et al. (2014), many early L-type subdwarfs occupy a distinct region of $J-K_S$ versus $J-W2$ color space blueward of the main clump of mostly M-type main sequence stars in $J-K_S$ color. Figure 6 shows a close-up view of this region along with the known early-type L subdwarfs from Kirkpatrick et al. (2014). We chose as subdwarf candidates those objects which lie blueward in $J-K_S$ color from the main clump of discoveries from this survey. Specifically, subdwarf candidates are those with a $J-W2$ color between 0.9 and 1.25 mag and a $J-K_S$ color less than 0.6 mag, a $J-W2$ color between 1.25 and 1.65 mag and a $J-K_S$ value less than $0.8\times(J-W2)-0.4$, or a $J-W2$ color between 1.65 and 1.9 mag and a $J-K_S$ color less than 0.92 mag, as shown in Figure 6. Of the 14 early-L subdwarfs from Kirkpatrick et al. (2014) in the figure, 9 meet the above criteria. We selected 31 subdwarf candidates based on their colors; they are listed in Table 8. While we include estimated spectral types for these objects in the table, we note that our spectral type estimation technique presented in the Appendix is predicated on the object in question having colors

Table 7
New Potential Nearby Objects

AllWISE Designation	Type[a] (photometric)	Dist. (pc)
J000856.39–281321.7	18.0	24–34
J001643.97+230426.5	18.9	23–31
J003338.45+282732.4	17.4	24–33
J010202.11+035541.4	18.9	23–31
J022721.93+235654.3	19.4	22–31
J030119.39–231921.1	20.5	24–33
J032309.12–590751.0	26.2	16–26
J034858.75–562017.8	22.6	24–33
J041743.13+241506.3	23.7	13–19
J053424.45+165255.0	15.4	18–25
J054455.54+063940.3	10.3	24–37
J060202.67+724235.4	18.7	23–31
J061429.77+383337.5	10.3	18–27
J083625.91–325034.5	5.2	22–35
J084254.56–061023.7	22.7	20–29
J085039.11–022154.3	16.3	21–30
J092740.70–500606.8	8.4	17–26
J093654.63–334620.5	9.9	22–34
J101944.62–391151.6	24.0	19–28
J105515.71–735611.3	7.4	8–12
J105811.69–583112.4	15.4	22–30
J111551.33–673135.5	8.4	13–21
J114117.13–790940.4	6.5	22–36
J121559.16–635351.8	7.0	22–35
J124138.43–643646.0	8.4	14–22
J130015.16–602417.2	6.0	16–26
J145640.16–535155.1	8.0	13–20
J150358.26–483505.0	8.3	19–30
J151029.95–604059.1	7.9	17–27
J154119.34–445055.8	8.0	22–34
J154209.42–515947.9	6.4	23–37
J164052.33–430750.7	5.8	12–20
J165057.66–221616.8	5.4	22–35
J165842.54+510334.9	13.7	23–33
J170234.91–670504.8	7.3	24–38
J171059.52–180108.7	5.2	24–37
J171105.08–275531.7	7.3	21–34
J171156.91–495441.1	8.1	20–31
J173551.56–820900.3	24.3	14–21
J174249.38–241101.6	7.6	10–15
J175546.92–340432.0	6.5	20–31
J183654.10–135926.2	8.7	20–31
J191011.03+563429.3	11.6	16–23
J201252.78+124633.3	6.5	17–26
J215620.63–532636.6	7.9	21–32
J225907.03–542036.9	7.0	17–28
WISE-only Sources		
J030919.70–501614.2	T7–T9	9–13
J133300.03–160754.4	T7–T9	17–24

Note.
[a] Numerical spectral type estimates (e.g., 5 = M5, 15 = L5, 25 = T5).

typical of a normal star or brown dwarf. Therefore, objects with colors distinct from those of normal late-type stars and brown dwarfs (such as subdwarfs) will likely be mistyped.

Besides being distinguishable in color space, subdwarfs often show kinematics distinct from that of the field population. These kinematic differences cause subdwarfs to stand out prominently in reduced proper motion diagrams, where the

Table 8
Color-selected Subdwarf Candidates

AllWISE Designation	$J-K_S$ (mag)	$J-W2$ (mag)	Type[a] (photometric)
J003449.93+551352.8	0.59 ± 0.08	1.11 ± 0.06	7.0
J011639.05–165420.5	0.84 ± 0.14	1.82 ± 0.08	15.8
J013012.66–104732.4	0.80 ± 0.13	1.63 ± 0.08	10.9
J025635.13–663443.9	0.84 ± 0.10	1.64 ± 0.06	10.2
J050750.72–034245.8	0.78 ± 0.11	1.60 ± 0.07	12.0
J052452.57+463202.9	0.58 ± 0.09	0.99 ± 0.06	8.2
J063228.30+264347.3	0.82 ± 0.09	1.60 ± 0.07	10.7
J094812.21–290329.5	0.69 ± 0.13	1.58 ± 0.07	11.8
J094904.92+023251.4	0.90 ± 0.20	1.68 ± 0.12	15.5
J101944.62–391151.6	0.30 ± 0.28	1.81 ± 0.10	24.0
J105617.57–465101.8	0.63 ± 0.14	1.31 ± 0.07	8.0
J112152.91–264937.3	0.59 ± 0.10	1.13 ± 0.06	6.4
J114553.61–250657.1	0.56 ± 0.17	1.19 ± 0.08	8.4
J120751.17+302808.9	0.79 ± 0.09	1.54 ± 0.06	10.6
J122355.12+551050.3	0.57 ± 0.17	1.45 ± 0.08	12.2
J124516.66+601607.5	0.58 ± 0.13	1.16 ± 0.07	9.4
J143559.87–443930.9	0.64 ± 0.11	1.34 ± 0.07	9.9
J143942.79–110045.4	0.80 ± 0.17	1.62 ± 0.10	11.8
J144056.64–222517.8	0.62 ± 0.10	1.30 ± 0.07	9.1
J155437.88–362534.4	0.68 ± 0.07	1.41 ± 0.05	9.8
J162046.30–485952.1	0.78 ± 0.04	1.60 ± 0.04	12.5
J163155.36+671549.3	0.70 ± 0.10	1.39 ± 0.06	9.2
J174006.68–733720.4	0.71 ± 0.17	1.49 ± 0.09	11.3
J180839.55+070021.7	0.79 ± 0.20	1.63 ± 0.12	14.7
J182010.20+202125.8	0.58 ± 0.09	1.01 ± 0.06	7.4
J213512.09–043155.0	0.84 ± 0.12	1.62 ± 0.06	10.4
J221126.37–192207.4	0.65 ± 0.16	1.42 ± 0.10	10.2
J221737.41–355242.7	0.64 ± 0.08	1.30 ± 0.06	10.3
J232656.09–181504.5	0.54 ± 0.11	1.24 ± 0.07	9.5
J234404.85–250042.2	0.86 ± 0.10	1.69 ± 0.07	11.8
J234812.74–530649.7	0.56 ± 0.10	1.06 ± 0.06	8.3

Note.
[a] Numerical spectral type estimates (e.g., 5 = M5, 15 = L5, 25 = T5).

reduced proper motion is defined as $H_m = m + 5\log(\mu) + 5$, where m is a particular photometric band and μ is the total proper motion. Figure 7 shows a reduced proper motion diagram for all of the discoveries from this *NEOWISE* search, as well as the known late-type subdwarfs from Kirkpatrick et al. (2014). We select candidate subdwarfs as either having H_J values greater than 18.7 mag and $J-W2$ values less than 1.8 or having H_J values greater than $\frac{3.8}{1.5} \times (J-W2) + 14.14$, as shown in the figure. These two selection criteria pick out 18 of the 21 known, late-type subdwarfs from Kirkpatrick et al. (2014) that have available J-band photometry and proper motion measurements. Thirty-one objects were selected as subdwarf candidates based on the reduced proper motion diagram positions. These subdwarf candidates are listed in Table 9. Four objects (WISEA J011639.05–165420.5, WISEA J094812.21–290329.5, WISEA J094904.92+023251.4, and WISEA J101944.62–391151.6) are common to both the reduced proper motion and color-selected subdwarf lists.

We have obtained follow-up spectra for five of these candidates (WISEA J011639.05–165420.5, WISEA J013012.66–104732.4, WISEA J114553.61–250657.1, WISEA J221126.37–192207.4, and WISEA J232656.09–181504.5). Each is discussed further in Section 5.2. We also observed one object that stood out in $J-K_S$ and $J-W2$ color space (WISEA J172602.92–034211.7; $J-K_S = 1.13$ mag, $J-W2 =$

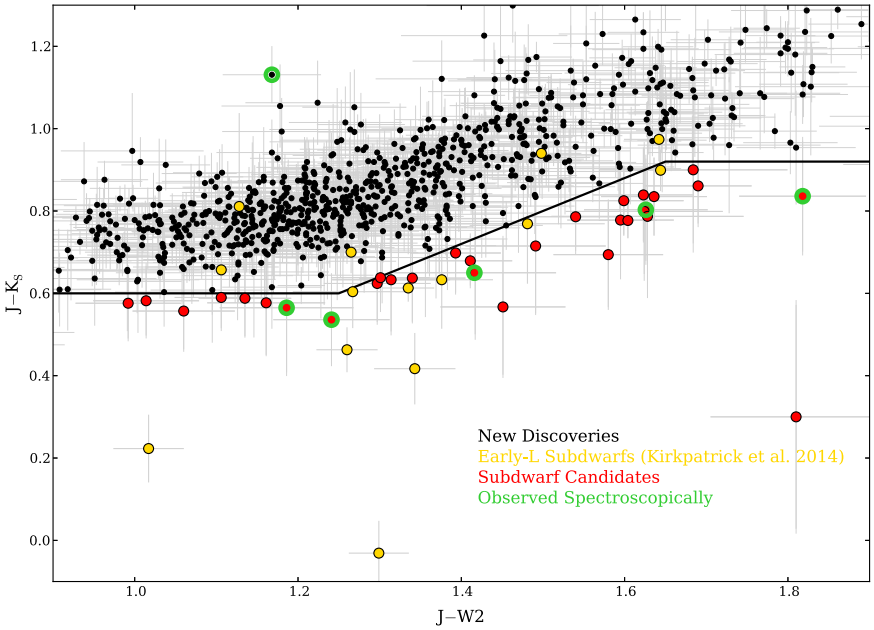

Figure 6. $J - K_S$ vs. $J - W2$ color–color diagram showing our color-selected subdwarf candidates. Early-L subdwarfs from Kirkpatrick et al. (2014) are plotted in gold. The solid line denotes our subdwarf color-candidate selection criteria. Objects that have been followed up spectroscopically are highlighted in green.

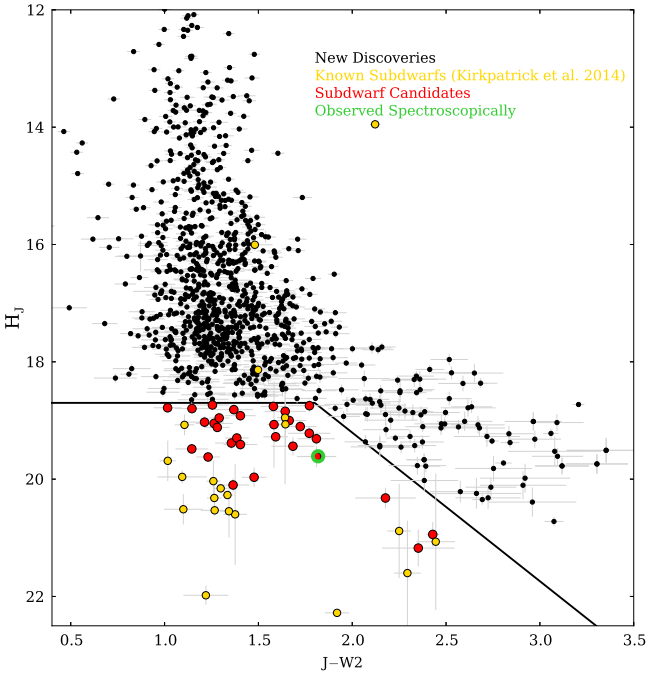

Figure 7. Reduced proper motion diagram in J for discoveries from this survey. The color-coding is the same as in Figure 6. The solid line denotes our subdwarf candidate selection criteria.

1.17 mag, see Figure 6) that turned out to be an early M-type subdwarf.

3.6. Comparison with Kirkpatrick et al. (2014) and Luhman (2014a) WISE Motion Surveys

Figure 8 shows a comparison of the total proper motions and *W2* magnitudes for all of the discoveries from this survey along with those from the *WISE* surveys of Kirkpatrick et al. (2014)

Table 9
Reduced Proper Motion Subdwarf Candidates

AllWISE Designation	H_J (mag)	$J - W2$ (mag)	Type[a] (photometric)
J000534.07–475033.0	19.41 ± 0.10	1.40 ± 0.09	5.0
J004555.13+795848.7	20.94 ± 0.21	2.43 ± 0.04	16.8
J010134.83+033616.0	19.97 ± 0.17	1.48 ± 0.07	7.0
J011639.05–165420.5	19.61 ± 0.09	1.82 ± 0.08	15.8
J013042.06–064705.1	19.38 ± 0.10	1.36 ± 0.09	6.3
J022045.20–550622.7	19.31 ± 0.10	1.81 ± 0.10	10.4
J025612.30+684752.6	18.92 ± 0.08	1.40 ± 0.08	6.8
J030421.32–394550.8	19.28 ± 0.10	1.59 ± 0.07	13.7
J032309.12–590751.0	21.18 ± 0.31	2.35 ± 0.19	26.2
J033346.88+385152.6	19.10 ± 0.08	1.72 ± 0.09	11.6
J044111.37+285338.2	19.48 ± 0.08	1.14 ± 0.09	<5.0
J055115.91+535607.9	20.10 ± 0.11	1.37 ± 0.09	5.5
J084903.52–511850.3	20.32 ± 0.17	2.18 ± 0.16	12.4
J092453.76+072306.0	19.05 ± 0.10	1.26 ± 0.10	5.9
J094812.21–290329.5	18.76 ± 0.07	1.58 ± 0.07	11.8
J094904.92+023251.4	19.44 ± 0.16	1.68 ± 0.12	15.5
J095230.79–282842.2	18.96 ± 0.07	1.29 ± 0.05	5.3
J101944.62–391151.6	19.62 ± 0.18	1.81 ± 0.10	24.0
J112158.76+004412.3	19.00 ± 0.09	1.66 ± 0.09	8.6
J121914.75+081027.0	19.03 ± 0.10	1.21 ± 0.10	<5.0
J122042.20+620528.3	19.12 ± 0.08	1.28 ± 0.06	6.3
J122402.69–714057.3	19.07 ± 0.73	1.58 ± 0.04	8.5
J123513.87–045146.5	18.80 ± 0.08	1.15 ± 0.09	5.1
J132240.10–331836.4	18.75 ± 0.10	1.77 ± 0.11	11.0
J133520.09–070849.3	19.22 ± 0.11	1.77 ± 0.11	12.3
J152548.25–374651.2	18.78 ± 0.07	1.02 ± 0.07	<5.0
J155225.22+095155.5	18.81 ± 0.10	1.37 ± 0.10	7.9
J160502.46–303205.9	18.74 ± 0.08	1.25 ± 0.09	<5.0
J171643.78+200616.1	19.62 ± 0.08	1.23 ± 0.06	<5.0
J171651.56–163912.5	19.30 ± 0.09	1.39 ± 0.06	5.9
J214338.47–170723.8	18.84 ± 0.10	1.64 ± 0.11	10.6

Note.
[a] Numerical spectral type estimates (e.g., 5 = M5, 15 = L5, 25 = T5).

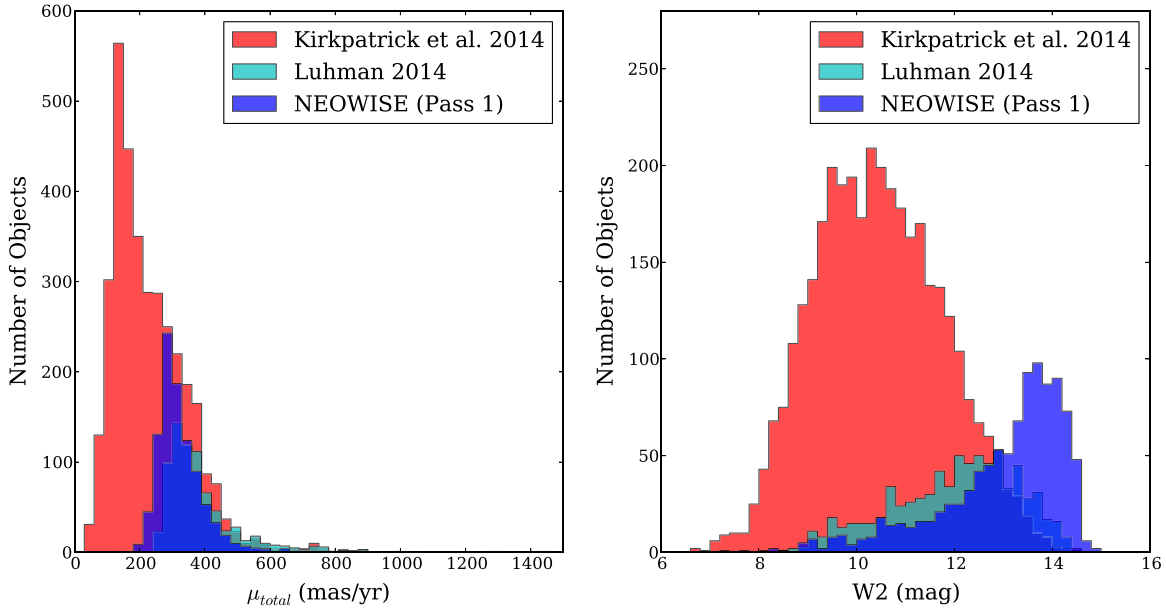

Figure 8. Distribution of discoveries from the *NEOWISE* proper motion survey, the AllWISE motion survey (Kirkpatrick et al. 2014), and the *WISE* motion survey of Luhman (2014a) in both total proper motion and *W2* magnitude.

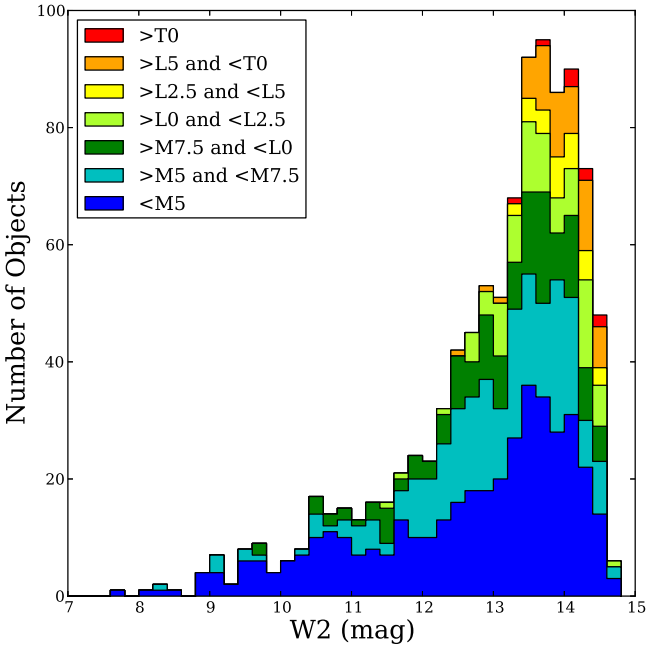

Figure 9. Distribution of discoveries from our *NEOWISE* proper motion survey in *W2* magnitude. The colors correspond to photometrically estimated spectral types.

and Luhman (2014a). While the AllWISE survey of Kirkpatrick et al. (2014) reported the largest number of new discoveries, they are by and large brighter and moving slower than those in the Luhman (2014a) and *NEOWISE* surveys. As seen in the left panel of the figure, the majority of the discoveries from this survey have total proper motions between 250 and 400 mas yr^{-1}, a similar result to the Luhman (2014a) survey, while the majority of the discoveries from the Kirkpatrick et al. (2014) AllWISE motion survey have total motions less than ~250 mas yr^{-1}, beyond the limit of our *NEOWISE* survey (see Section 2).

Table 10
New >L7 Brown Dwarf Candidates

AllWISE Designation	Type[a] (photometric)
J000430.66–260402.3	20.5
J000536.63–263311.8	17.1
J000856.39–281321.7	18.0
J001643.97+230426.5	18.9
J003338.45+282732.4	17.4
J010202.11+035541.4	18.9
J010631.20–231415.1	18.2
J013525.38+020518.2	17.7
J022721.93+235654.3	19.4
J024502.87–744519.3	17.2
J030119.39–231921.1	20.5
J031627.79+265027.5	19.0
J032309.12–590751.0	26.2
J032744.41–620336.3	17.7
J032838.73+015517.7	18.5
J034409.71+013641.5	19.1
J034858.75–562017.8	22.6
J041318.68+210326.5	17.7
J041743.13+241506.3	23.7
J051526.68–230954.2	17.1
J060202.67+724235.4	18.7
J062858.69+345249.2	17.2
J063552.52+514820.4	17.4
J084254.56–061023.7	22.7
J101944.62–391151.6	24.0
J103534.63–071148.2	17.7
J105131.36–144017.2	19.4
J135501.90–825838.9	17.1
J141127.86–481150.6	20.5
J172120.69+464025.9	18.2
J173551.56–820900.3	24.3
J192714.29+383754.2	17.0
J211157.84–521111.3	19.7
J211219.83–491717.0	17.8
J223343.53–133140.9	17.2
J223444.44–230916.1	17.4
J224931.10–162759.6	17.1
J230329.45+315022.7	18.3

Note.
[a] Numerical spectral type estimates (e.g., 5 = M5, 15 = L5, 25 = T5).

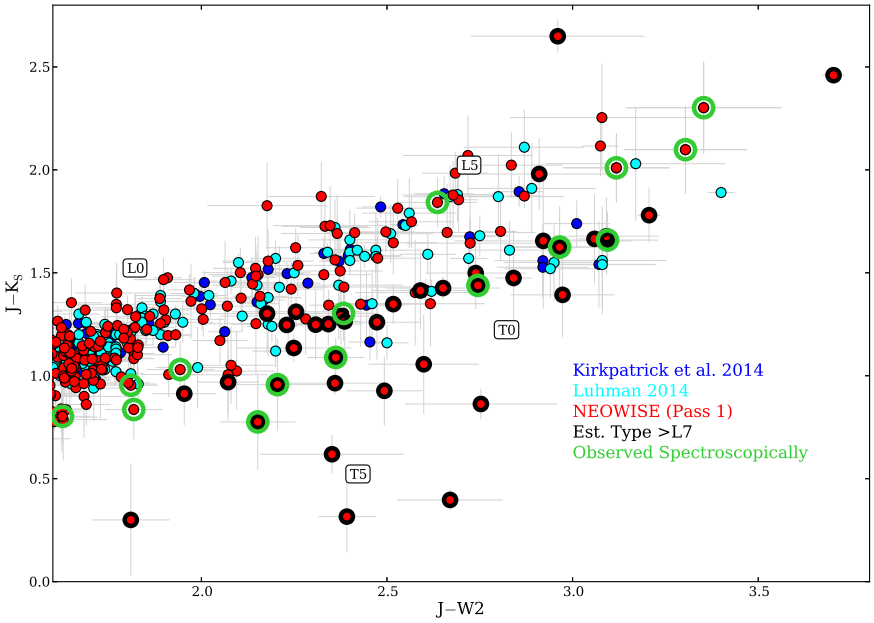

Figure 10. $J - K_S$ vs. $J - W2$ color–color diagram showing our new L and T type discoveries from Luhman (2014a), Kirkpatrick et al. (2014), and this survey. Discoveries from this survey with estimated spectral types later than L7 are highlighted in black.

Table 11
Observations

AllWISE Designation	Sp. Type	Type[a] (photometric)	Dist. (pc)	V_{tan} (km s^{-1})	Obs. Date (UT)	Exp. Time[b] (s)
			IRTF/SpeX			
J000627.85+185728.8	L7	16.1	31–35	43–50	2015 Jun 27	1200
J001643.97+230426.5	T0	18.9	23–27	42–50	2015 Jul 19	1200
J003338.45+282732.4	L3 (blue)	17.4	38–44	59–69	2015 Jun 27	1200
J010202.11+035541.4	L9	18.9	25–29	44–52	2015 Jul 19	1200
J011639.05–165420.5	d/sdM8.5	15.8	78–92	213–252	2015 Jun 27	1200
J013012.66–104732.4	d/sdM8.5	10.9	78–92	130–155	2015 Feb 26	1200
J114553.61–250657.1	d/sdM7	8.4	107–128	129–156	2015 May 9	1200
J120035.40–283657.5	T0	16.7	22–26	56–58	2015 Jan 28	960
J122221.95–213948.6	L6	14.4	28–33	45–54	2015 May 8	1200
J130729.56–055815.4	L8 (sl. blue)	16.9	26–30	45–53	2015 Jan 28	1440
J144033.28–080406.9	L2 (blue)	15.2	50–58	78–92	2015 May 9	1200
J170726.69+545109.3	L1 (blue)	13.0	59–68	84–97	2015 Jun 27	1200
J172120.69+464025.9	T0: (pec)	18.2	26–30	33–39	2015 Jun 27	1200
J205202.06–204313.0	L8 (sl. blue)	15.9	27–31	50–58	2015 Jun 27	1200
J223343.53–133140.9	T2 (blue)	17.2	26–30	39–46	2015 Jul 19	1200
J230329.45+315022.7	T2 (blue)	18.3	24–28	32–38	2015 Jun 27	1200
			Palomar/DoubleSpec			
J172602.92–034211.7	sdM1.5	5.3	95–151	126–201	2015 Sep 1	2400,2460
J221126.37–192207.4	M5/sdM6	10.2	65–99	100–153	2015 Sep 1	2400,2460
J232656.09–181504.5	M5	9.5	62–97	89–137	2015 Sep 1	2400,2460

Notes.
[a] Numerical spectral type estimates (e.g., 5 = M5, 15 = L5, 25 = T5).
[b] The two exposure times listed for Palomar/DoubleSpec observations refer to the blue and red sides of the spectrograph.

As seen in the right panel of the figure, our *NEOWISE* motion survey has found significantly more objects at fainter magnitudes than the *WISE* surveys of Kirkpatrick et al. (2014) and Luhman (2014a). Figure 9 shows the same *NEOWISE* histogram from the right panel of Figure 8 broken up by estimated spectral type. As seen in the figure, almost every one of our new L and T dwarf candidates is contained within the fainter *W2* magnitude bins. Of the 187 *NEOWISE* discoveries with estimated spectral types later than L0, 170 (~91%) have *W2* magnitudes greater than 13.

The enhanced sensitivity of our survey to fainter high proper motion objects compared to the previous *WISE* motion surveys

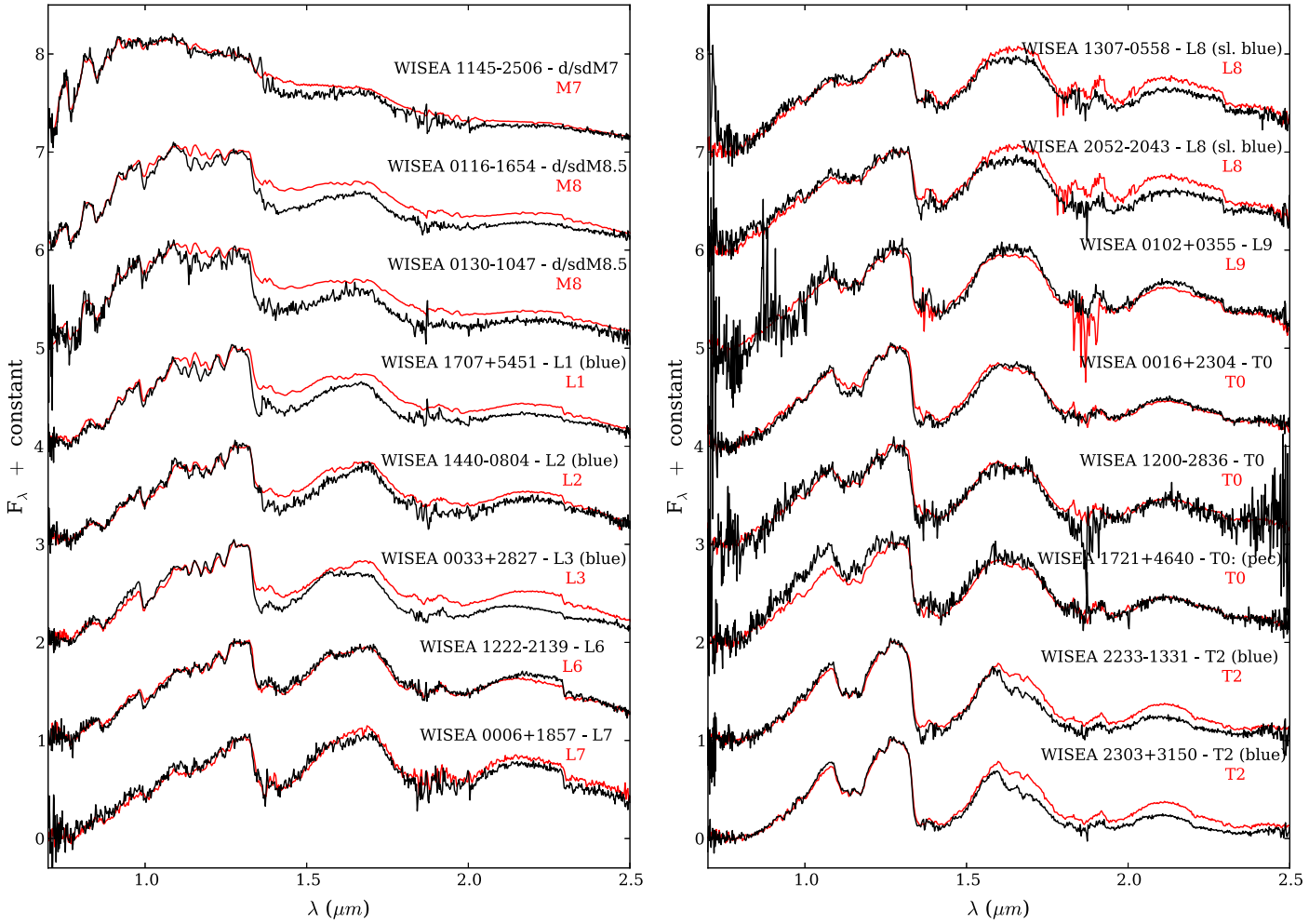

Figure 11. IRTF/SpeX spectra of new M, L, and T dwarfs compared to near-infrared spectral standards (red). All spectra are normalized at 1.28 μm. The spectral standards are: VB 8 (M7; Burgasser et al. 2008) VB 10 (M8; Burgasser et al. 2004), 2MASSW J2130446–084520 (L1; Kirkpatrick et al. 2010), Kelu−1 (L2; Burgasser et al. 2007), 2MASSW J1506544+132106 (L3; Burgasser et al. 2007), 2MASSI J1010148–040649 (L6; Reid et al. 2006), 2MASSI J0103320+193536 (L7; Cruz et al. 2004), 2MASSW J1632291+190441 (L8; Burgasser et al. 2007), DENIS-P J0255–4700 (L9; Burgasser et al. 2006), SDSS J120747.17+024424.8 (T0; Looper et al. 2007), and SDSSp J125453.90–012247.4 (T2; Burgasser et al. 2004).

has allowed us to identify several new brown dwarfs with estimated spectral types around and later than the L/T transition. Figure 10 shows a close-up view of the region of $J - K_S$ versus $J - W2$ color space occupied by L and T dwarfs. In addition to the new discoveries from this survey, we also show the discoveries from the Luhman (2014a) and Kirkpatrick et al. (2014) surveys. The figure shows that all of the surveys have identified several objects in the early to mid-L spectral type range; however, only our *NEOWISE* survey identified new objects extending down into the mid-T dwarf color range. Note that objects without 2MASS counterparts are not included in this figure. Only one confirmed high proper motion object without a 2MASS counterpart was identified in the Luhman (2014a) and Kirkpatrick et al. (2014) surveys (WISE J085510.83–071442.5). There are two such objects in our discovery list (see Sections 3.1 and 3.4). All objects with estimated spectral types later than L7 are listed in Table 10. We chose L7 to create this list because of the tendency of our classification program to mistype early T dwarfs as mid-Ls. All 39 objects with estimated spectral types later than L7 are highlighted in Figure 10. Follow-up spectroscopic observations for six of these objects (WISEA J001643.97+230426.5, WISEA J003338.45+282732.4, WISEA J010202.11+035541.4, WISEA J172120.69+464025.9, WISEA J223343.53–133140.9, and WISEA J230329.45+315022.7) are discussed in Section 5.2. Spectral types for all of these objects are determined to be later than L7, with the exception of WISEA J003338.45+282732.4, a blue L3.

We can also place constraints on the existence of additional extremely cold, nearby WISE J085510.83–071442.5-type objects. WISE J085510.83–071442.5 has a *W2* magnitude of 14.02 ± 0.05 at a distance of 2.02 pc (Luhman & Esplin 2014). Using our *W2* survey limit 14.5, we can rule out the existence of additional J085510.83–071442.5-type objects with total proper motions between 0.25 and 15″ yr^{-1} out to ∼2.9 pc. Using the absolute magnitude–spectral type relations from Dupuy & Liu (2012) and our *W2* survey limit, we can also rule out the existence of additional Y0 and Y1 type dwarfs with proper motions between 0.″25 yr^{-1} and 15″ yr^{-1} out to distances of ∼11.5 pc and ∼9.5 pc, respectively. A substantial increase in survey depth will be needed to place further constraints on the existence of such late-type objects in the Solar neighborhood.

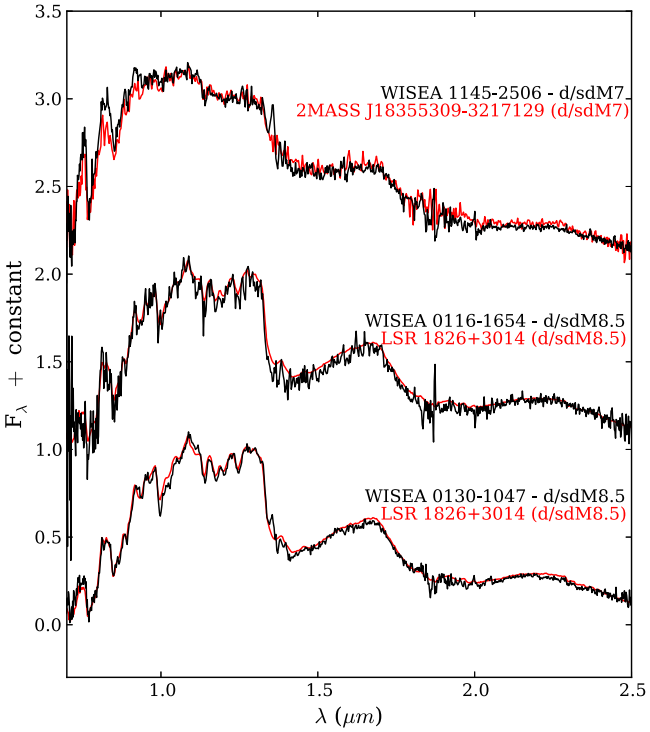

Figure 12. IRTF/SpeX spectra of 3 late-M subdwarf candidates. Comparison spectra are 2MASS J18355309–3217129 (d/sdM7—Kirkpatrick et al. 2010) and LSR 1826+3014 (d/sdM8.5—Burgasser et al. 2004).

4. FOLLOW-UP OBSERVATIONS

4.1. IRTF/SpeX

Low-resolution ($\lambda/\Delta\lambda$ = 75–120) spectra were acquired for several sources with the upgraded SpeX spectrograph (Rayner et al. 2003) at the 3 m NASA Infrared Telescope Facility (IRTF) on Mauna Kea. All observations were conducted using the prism mode. A series of exposures was taken using an ABBA nod pattern along the 15″ long slit for each object. A0V stars were observed at similar airmasses for telluric correction purposes. Data for all objects were reduced using the SpeXtool reduction package (Vacca et al. 2003; Cushing et al. 2004). A summary of all IRTF/SpeX observations is given in Table 11.

4.2. Palomar/DoubleSpec

Three targets were observed with the Double Spectrograph on the Hale 5 m telescope on the night of UT 2015 September 07. For the blue side of the spectrograph, we employed a 600 lines mm^{-1} grating blazed at 4000 Å for a total range of spectral coverage from 4015 to 7085 Å. For the red side of the spectrograph, we used a 600 lines mm^{-1} grating blazed at 10000 Å for a total range of spectral coverage from 6545 to 9910 Å. The overlapping regions were used to create one continuous spectrum across the entire range. The flux standard used was Wolf 1346, which was bootstrapped to the flux calibration of Hamuy et al. (1994) using the standard Hiltner 600, both of which had been observed in an earlier run with the same setup on UT 2014 September 27. Data were reduced using standard reduction procedures.

5. ANALYSIS

5.1. Spectral Classification

We determine spectral types for all near-infrared spectra following the method outlined in the appendix of Schneider et al. (2014). Comparisons of each acquired spectrum with its best matching near-infrared spectral standard from the Spex Prism Spectral Library (Burgasser 2014)[7] are shown in Figure 11. Spectral types are provided in Table 11. We also include the spectral type estimates from Table 1 for comparison. It should come as no surprise that the estimated spectral types differ significantly from the actual spectral types for these objects because many are poor matches to the spectral standards and occupy unique regions of color space (see Figures 5, 6, 10, and 11 and Section 5.2). The three L dwarfs that match well at all near-infrared wavelengths with their corresponding spectral standard (WISEA J122221.95–213948.6, WISEA J000627.85+185728.8, and WISEA J010202.11+035541.4) all have photometric spectral type estimates within ∼1.5 subtypes of their actual type. While the two new T0 dwarfs (WISEA J001643.97+230426.5 and WISE J120035.40–283657.5) are good matches to the T0 standard, their estimated types are several subtypes earlier (18.9 and 16.7, respectively). This is not unexpected, as early T dwarfs typically have photometric spectral type estimates earlier than their actual type using our classification method (see the Appendix). We estimate the distance to each observed object using the spectral types determined from the comparison with spectral standards, *W2* magnitudes, and the absolute magnitude–spectral type relations from Dupuy & Liu (2012) and provide distance ranges in Table 11 using a ±0.5 subtype uncertainty and photometric uncertainties.

All optical spectra were classified based on the classification system of Kirkpatrick et al. (1991) for normal M dwarfs or the subdwarf classification scheme of Lépine et al. (2007).

5.2. Individual Objects of Note

WISEA J001643.97+230426.5 and WISEA J010202.11+035541.4: Both WISEA J001643.97+230426.5 and WISEA J010202.11+035541.4 were singled out as potentially nearby (Table 7) and late-type (Table 10). Both objects have photometric type estimates similar to their actual spectral types (see Table 9), and therefore have similar spectral type distance estimates. Both of these brown dwarfs are estimated to be within ∼30 pc.

WISEA J011639.05–165420.5, WISEA J013012.66–104732.4, and WISEA J114553.61–250657.1: All three of these objects were chosen for follow-up because they have colors indicative of being late M-type subdwarfs (see Figure 6 and Table 8). WISEA J011639.05–165420.5 was also chosen as a subdwarf candidate from its placement on the reduced proper motion diagram in Figure 7. While each of these three objects match reasonably well to either the M7 or M8 near-infrared spectral standard in the J-band, they are all poor matches at H and K because they are much bluer than the standards. This is a characteristic typical of late-type subdwarfs. In Figure 12 we show the near-infrared spectra of these three objects compared with subdwarf spectra from the Spex Prism Spectral Library (Burgasser 2014). As seen in the figure, WISEA J114553.61–250657.1 closely resembles

[7] http://pono.ucsd.edu/~adam/browndwarfs/spexprism/library.html

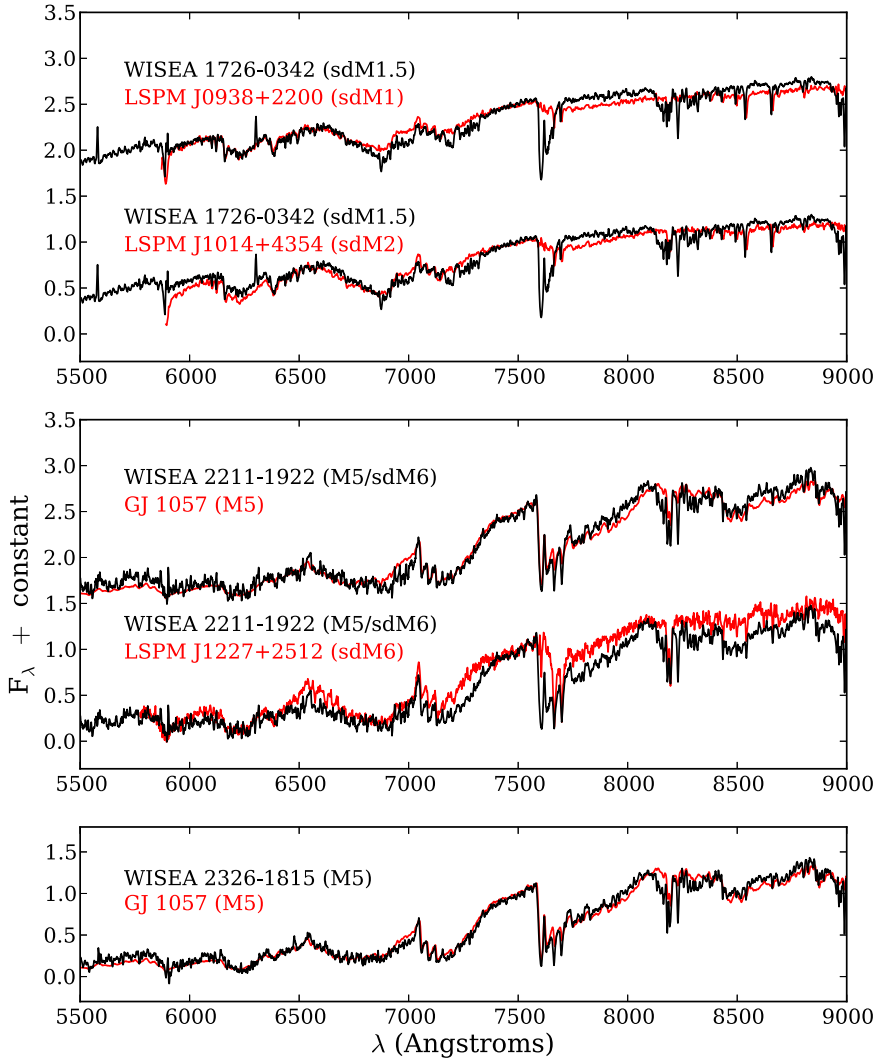

Figure 13. Palomar/DoubleSpec optical spectra (black) compared to dwarf and subdwarf spectral standards (red). All spectra are normalized at 7500 Å. The spectral standards are: LSPM J0938+2200 (sdM1; Lépine et al. 2007), LSPM J1014+4354 (sdM2; Lépine et al. 2007), GJ 1057 (M5; Kirkpatrick et al. 1997), and LSPM J1227+2512 (sdM7; Lépine et al. 2007). Note that the subdwarf standards from Lépine et al. (2007) are corrected for telluric absorption and our Palomar DoubleSpec spectra are not.

2MASS J18355309–3217129, which is classified as d/sdM7 in Kirkpatrick et al. (2010). The figure also shows that both WISEA J011639.05–165420.5 and WISEA J013012.66–104732.4 are similar to LSR 1826+3014, classified as d/sdM8.5 in Burgasser et al. (2004). While the relations from Dupuy & Liu (2012) are designed for normal objects, not subdwarfs, we still use the relations for these three objects only as preliminary distance estimates. Given their new spectral classifications, we estimate distance ranges for WISEA J011639.05–165420.5, WISEA J013012.66–104732.4, and WISEA J114553.61–250657.1 of 78–92, 78–92, and 107–128 pc, respectively. Using these distance estimates, along with their proper motions, we consider whether any of these objects are part of the thick disk/halo population based on their tangential velocities ($V_{\rm tan}$). We find $V_{\rm tan}$ ranges of 213–252, 130–155, and 129–156 km s^{-1}, which do indeed point toward membership in the thick disk/halo population, as Faherty et al. (2009) find a median tangential velocity of 26 km s^{-1} with a dispersion of 19 km s^{-1} for late-M dwarfs. Membership in the thick disk/halo is not surprising given their blue near-infrared colors and subdwarf spectral classifications. Future optical spectroscopy could confirm each of these object's low metallicity and their subdwarf classification.

WISEA J003338.45+282732.4, WISEA J144033.28–080406.9, and WISEA J170726.69+545109.3: WISEA J003338.45+282732.4 was identified as a potentially nearby object (Table 7) and as a potential T dwarf (Table 10). All three of these objects match well to early L spectral standards at J, but are much bluer overall. Surface gravity and/or low metallicity are thought to account for the blue color of blue L dwarfs, which is supported by their kinematics (Faherty et al. 2009). We classify each of these three objects as early-type blue L dwarfs. We calculate $V_{\rm tan}$ ranges of 59–69, 78–92, and 84–97 km s^{-1} for WISEA J003338.45+282732.4, WISEA J144033.28–080406.9, and WISEA J170726.69+545109.3, respectively, using their photometric distance estimates. These values are higher than the median tangential velocities for L dwarfs of ~30 km s^{-1} found in previous studies (Schmidt et al. 2010; Faherty et al. 2012). Optical spectroscopy would be able to determine if the blue nature of these L dwarfs is due to low-metallicity.

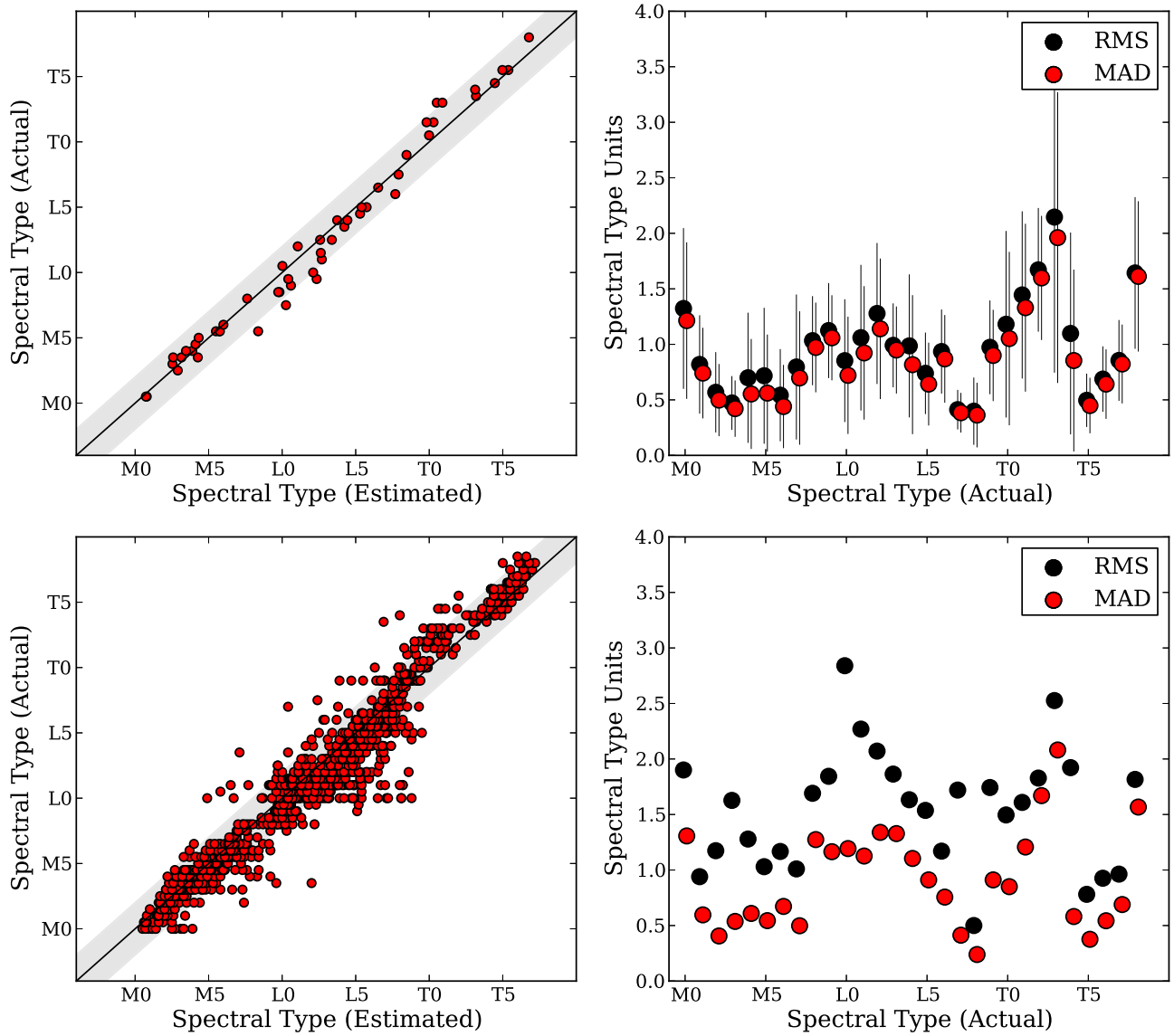

Figure 14. Top left: the actual vs. estimated spectral types for a test sample comprising of 10% of the training sample using the k-Nearest Neighbors classification algorithm. The gray bar indicates ±2 subtypes. Top right: the rms and the median of absolute differences (MAD—defined in Equation (1)) as a function of spectral type for the 1000 simulations. Bottom left: the actual vs. estimated spectral types for every M, L, and T dwarf with a near-infrared spectral type from DwarfArchives. The gray bar indicates ±2 subtypes. Bottom right: the rms and the MAD as a function of spectral type for the entire M, L, and T dwarf sample from DwarfArchives.

WISEA J130729.56–055815.4 and WISEA J205202.06–204313.0: Both of these objects are slightly bluer than the L8 spectral standard. We classify each as L8 (sl. blue).

WISEA J172120.69+464025.9: WISEA J172120.69+464025.9 was selected as a potential late-type brown dwarf (Table 10). This object does not match well with any of the spectral standards, but generally displays the overall shape of a T0. We classify this object as T0: (pec). We investigated spectral binarity as a possible explanation for this object's unusual spectrum (e.g., Burgasser 2007; Bardalez Gagliuffi et al. 2014), but could not find a satisfactory fit.

WISEA J223343.53–133140.9 and WISEA J230329.45+315022.7: WISEA J223343.53–133140.9 and WISEA J230329.45+315022.7 were both selected as potential late-type brown dwarfs (Table 10). Both of these objects are excellent matches to the T2 spectral standard at J; however, both are significantly bluer than the standards. We therefore classify them at T2 (blue).

WISEA J172602.92–034211.7: This object was chosen for follow-up spectroscopy because it stood out prominently in color space, with $J - K_S$ and $J - W2$ values of 1.13 and 1.17 mag, respectively (see Figure 6). Optical spectroscopy revealed this object to be a metal-poor early M-type star (Figure 13). Comparison with the sdM standards of Lépine et al. (2007) show good agreement with the sdM1 and sdM2 standards. We therefore classify WISEA J172602.92–034211.7 as an sdM1.5.

WISEA J221126.37–192207.4 and WISEA J232656.09–181504.5: These objects are color-selected subdwarf candidates (see Table 8). WISEA J232656.09–181504.5 may be slightly metal-poor, but is overall a good match to the normal M5 standard (Figure 13) and therefore classified as M5. Figure 13 also shows that WISEA J221126.37–192207.4 matches fairly well with the M5 standard. However, this object's spectrum does show slightly enhanced CaH absorption around 7000 Å, which is typical of M subdwarfs (Lépine

et al. 2007). We also show in Figure 13 a comparison with the sdM6 standard, which matches fairly well. We measure a $\zeta_{TiO/CaH}$ metallicity index of 0.865, slightly above the cutoff value between normal dwarfs and subdwarfs of 0.825 given in Lépine et al. (2007). We conservatively give WISEA J221126.37–192207.4 a spectral type of M5/sdM6.

6. CONCLUSION

We have conducted a survey for high proper motion objects using the first sky pass of *NEOWISE* and the AllWISE catalog, identifying over 20,000 high proper motion objects, over 1,000 of which are new discoveries. Through an analysis of 2MASS and AllWISE colors and estimated spectral types, we have picked out a number of appealing candidates identified as being nearby objects, subdwarfs, or late-type brown dwarfs, several of which have been confirmed with near-infrared or optical spectroscopy. The success of this survey, and the previous motion surveys of Luhman (2014a) and Kirkpatrick et al. (2014), demonstrates the effectiveness of using data from the *WISE* telescope to identify previously overlooked objects of scientific interest. The foremost limiting factor for these surveys has been the depth at which objects with large motions can be readily identified. A future catalog produced from co-adding the *NEOWISE* single frames would significantly increase the survey volume of this type of effort, and would only enlarge the already substantial legacy of the *WISE* telescope.

The authors wish to thank Sébastian Lépine for graciously providing us with subdwarf standard spectra. This publication makes use of data products from the *Wide-field Infrared Survey Explorer*, which is a joint project of the University of California, Los Angeles, and the Jet Propulsion Laboratory/California Institute of Technology, and *NEOWISE*, which is a project of the Jet Propulsion Laboratory/California Institute of Technology. *WISE* and *NEOWISE* are funded by the National Aeronautics and Space Administration. This research has benefited from the M, L, T, and Y dwarf compendium housed at DwarfArchives.org. This research has made use of the VizieR catalog access tool and SIMBAD database operated at, CDS, Strasbourg, France. Funding for SDSS-III has been provided by the Alfred P. Sloan Foundation, the Participating Institutions, the National Science Foundation, and the U.S. Department of Energy Office of Science. The SDSS-III web site is http://www.sdss3.org/. SDSS-III is managed by the Astrophysical Research Consortium for the Participating Institutions of the SDSS-III Collaboration including the University of Arizona, the Brazilian Participation Group, Brookhaven National Laboratory, Carnegie Mellon University, University of Florida, the French Participation Group, the German Participation Group, Harvard University, the Instituto de Astrofisica de Canarias, the Michigan State/Notre Dame/JINA Participation Group, Johns Hopkins University, Lawrence Berkeley National Laboratory, Max Planck Institute for Astrophysics, Max Planck Institute for Extraterrestrial Physics, New Mexico State University, New York University, Ohio State University, Pennsylvania State University, University of Portsmouth, Princeton University, the Spanish Participation Group, University of Tokyo, University of Utah, Vanderbilt University, University of Virginia, University of Washington, and Yale University.

APPENDIX
PHOTOMETRIC SPECTRAL TYPE ESTIMATES

In order to prioritize the most interesting objects from our list of new discoveries for follow-up observations, we endeavored to find a way to accurately estimate approximate spectral types for each object using solely 2MASS and AllWISE photometry. While previous studies have attempted photometric typing, mainly using color-spectral type polynomial relations (e.g., Luhman & Sheppard 2014 and Skrzypek et al. 2015), machine learning algorithms are an alternative tool to use to accomplish this type of classification. For this work, we utilized k-NN algorithm using code available from the scikit-learn project (Pedregosa et al. 2011). The k-NN algorithm classifies by identifying the closest training data points within the space being examined. For a test sample, the Euclidean distance is calculated for each member of the comparison data set. The k value determines how many training data points are selected. The test sample is then classified into the training set that is most common among its k nearest neighbors. This requires a well defined training set of known objects with known spectral types. We used an updated list of M, L, and T dwarfs from DwarfArchives.org with near-infrared spectral types (C. Gelino 2015, private communication). For each object from the DwarfArchives list, we found its corresponding 2MASS and AllWISE catalog entries, retaining only those objects that had both. In order to ensure that the estimated spectral classifications are not biased toward spectral classes for which there is a larger population of objects, we limit the training set to have a maximum of 10 objects per half spectral type bin. Objects included in the training set were preferentially chosen to have the smallest photometric uncertainties.

We evaluate the accuracy of photometrically classifying objects using the k-NN algorithm using two different test sets. For the first, we randomly selected 10% of objects from the training set. For the second, we use the entire list of M, L, and T dwarfs from the DwarfArchives list. We then evaluate for each object in each test sample the probability of belonging to every spectral class for every possible color–color combination using 2MASS J, H, and K_S and AllWISE $W1$ and $W2$ magnitudes (45 total). A final spectral type estimate for each object in the test sample is determined by summing the product of the probabilities for each spectral type and the numbered index for that spectral type (e.g., M5 = 5, L5 = 15, T5 = 25). We repeat the procedure for the first test set 1000 times, and test the accuracy by using two different metrics; the rms and the median of the absolute differences (MAD), which we use in an attempt to account for outliers, defined as

$$\text{median}|SpT_{\text{actual}} - SpT_{\text{estimated}}|, \quad (1)$$

where SpT_{actual} is the near-infrared spectral type from DwarfArchives, and $SpT_{\text{estimated}}$ is the spectral type determined by the algorithm. A comparison of the estimated spectral types versus the actual spectral types for one run of the 10% sample is shown in the top left panel of Figure 14. The average and standard deviation of rms and MAD values for the entire simulation of 10% test samples are 1.14 ± 0.15 and 0.67 ± 0.10 subtypes, respectively. However, the rms and MAD values are spectral-type dependent, as shown in the right panel of Figure 14. Almost all objects have estimated spectral types within 1.5 subtypes of their actual type. Early T dwarfs (T2s and T3s) are consistently classified as several subtypes

earlier than their actual type. We suspect this is because mid-L dwarfs and early T dwarfs share similar near- and mid-infrared colors (Kirkpatrick et al. 2011). For the entire list of M, L, and T dwarfs from DwarfArchives, we find slightly larger rms and MAD values of 1.75 and 0.87, respectively. A comparison of the estimated spectral types versus the actual spectral types for this entire sample is shown in the bottom left panel of Figure 14. We see large rms values for very early L dwarfs, approaching values as high as ~3 subtypes for L0. This is clearly due to excess outliers, as the MAD values are not so extreme. These outliers may be actual photometric outliers, or potentially mistyped L dwarfs. We see the same peak around T3 as seen in the 10% sample, most likely for the same reasons. For the vast majority of objects in the entire DwarfArchive near-infrared spectral type catalog, spectral types are accurate to within ±2 subtypes.

To compare our results with those that use polynomial relations, we evaluate our classifications using the same robust estimator as that used in Skrzypek et al. (2015), namely

$$\sigma = \frac{\sum_{i=1}^{N} |\Delta t|}{N} \frac{\sqrt{2\pi}}{2}. \quad (2)$$

For the entire DwarfArchive list, we find $\sigma_M = 1.2$, $\sigma_L = 1.8$, and $\sigma_T = 1.4$. These values are similar to those found for the polynomial relations in Skrzypek et al. (2015) of $\sigma_L = 1.5$ and $\sigma_T = 1.2$. However, note that our method uses only JHKW1W2 photometry, while the method in Skrzypek et al. (2015) uses izYJHKW1W2, when available.

REFERENCES

Ammons, S. M., Robinson, S. E., Strader, J., et al. 2006, ApJ, 638, 1004
Artigau, É., Radigan, J., Folkes, S., et al. 2010, ApJL, 718, L38
Bardalez Gagliuffi, D. C., Burgasser, A. J., Gelino, C. R., et al. 2014, ApJ, 794, 143
Barnard, E. E. 1916, AJ, 29, 181
Bihain, G., Scholz, R.-D., Storm, J., & Schnurr, O. 2013, A&A, 557, A43
Boyd, M. R., Henry, T. J., Jao, W.-C., Subasavage, J. P., & Hambly, N. C. 2011, AJ, 142, 92
Burgasser, A. J. 2007, ApJ, 659, 655
Burgasser, A. J. 2014, in Astronomical Society of India Conf. Ser. 11, International Workshop on Stellar Spectral Libraries, ed. H. P. Singh, P. Prugniel, & I. Vauglin, 7
Burgasser, A. J., Geballe, T. R., Leggett, S. K., Kirkpatrick, J. D., & Golimowski, D. A. 2006, ApJ, 637, 1067
Burgasser, A. J., Liu, M. C., Ireland, M. J., Cruz, K. L., & Dupuy, T. J. 2008, ApJ, 681, 579
Burgasser, A. J., Looper, D. L., Kirkpatrick, J. D., & Liu, M. C. 2007, ApJ, 658, 557
Burgasser, A. J., McElwain, M. W., Kirkpatrick, J. D., et al. 2004, AJ, 127, 2856
Cruz, K. L., Burgasser, A. J., Reid, I. N., & Liebert, J. 2004, ApJL, 604, L61
Cushing, M. C., Vacca, W. D., & Rayner, J. T. 2004, PASP, 116, 362
Deacon, N. R., & Hambly, N. C. 2007, A&A, 468, 163
Deacon, N. R., Hambly, N. C., King, R. R., & McCaughrean, M. J. 2009, MNRAS, 394, 857
Deacon, N. R., Liu, M. C., Magnier, E. A., et al. 2011, AJ, 142, 77
Dupuy, T. J., & Liu, M. C. 2012, ApJS, 201, 19
Faherty, J. K., Burgasser, A. J., Cruz, K. L., et al. 2009, AJ, 137, 1
Faherty, J. K., Burgasser, A. J., Walter, F. M., et al. 2012, ApJ, 752, 56
Gagné, J., Lafrenière, D., Doyon, R., Malo, L., & Artigau, É. 2015, ApJ, 798, 73
Gianninas, A., Bergeron, P., & Ruiz, M. T. 2011, ApJ, 743, 138
Gizis, J. E., Burgasser, A. J., Faherty, J. K., Castro, P. J., & Shara, M. M. 2011, AJ, 142, 171
Gliese, W., & Jahreiß, H. 1991, Preliminary Version of the Third Catalogue of Nearby Stars, Tech. Rep., ed. L. E. Brotzmann & S. E. Gesser (Greenbelt, MD: NASA Astronomical Data Center, Goddard Space Flight Center)
Hamuy, M., Suntzeff, N. B., Heathcote, S. R., et al. 1994, PASP, 106, 566
Hoffleit, D., & Jaschek, C. 1991, The Bright Star Catalogue (5th ed.; New Haven, CT: Yale Univ. Observatory)
Kirkpatrick, J. D., Beichman, C. A., & Skrutskie, M. F. 1997, ApJ, 476, 311
Kirkpatrick, J. D., Cushing, M. C., Gelino, C. R., et al. 2011, ApJS, 197, 19
Kirkpatrick, J. D., Gelino, C. R., Cushing, M. C., et al. 2012, ApJ, 753, 156
Kirkpatrick, J. D., Henry, T. J., & McCarthy, D. W., Jr. 1991, ApJS, 77, 417
Kirkpatrick, J. D., Looper, D. L., Burgasser, A. J., et al. 2010, ApJS, 190, 100
Kirkpatrick, J. D., Reid, I. N., Liebert, J., et al. 1999, ApJ, 519, 802
Kirkpatrick, J. D., Schneider, A., Fajardo-Acosta, S., et al. 2014, ApJ, 783, 122
Kordopatis, G., Gilmore, G., Steinmetz, M., et al. 2013, AJ, 146, 134
Lee, S.-G. 1984, AJ, 89, 702
Leggett, S. K., Geballe, T. R., Fan, X., et al. 2000, ApJL, 536, L35
Lépine, S., & Bongiorno, B. 2007, AJ, 133, 889
Lépine, S., Rich, R. M., & Shara, M. M. 2007, ApJ, 669, 1235
Lépine, S., & Shara, M. M. 2005, AJ, 129, 1483
Liu, M. C., Deacon, N. R., Magnier, E. A., et al. 2011, ApJL, 740, L32
Looper, D. L., Kirkpatrick, J. D., & Burgasser, A. J. 2007, AJ, 134, 1162
Luhman, K. L. 2013, ApJL, 767, L1
Luhman, K. L. 2014a, ApJ, 781, 4
Luhman, K. L. 2014b, ApJL, 786, L18
Luhman, K. L., & Esplin, T. L. 2014, ApJ, 796, 6
Luhman, K. L., & Sheppard, S. S. 2014, ApJ, 787, 126
Mainzer, A., Bauer, J., Cutri, R. M., et al. 2014, ApJ, 792, 30
Metchev, S. A., Kirkpatrick, J. D., Berriman, G. B., & Looper, D. 2008, ApJ, 676, 1281
Pedregosa, F., Varoquaux, G., Gramfort, A., et al. 2011, JMLR, 12, 2825
Pokorny, R. S., Jones, H. R. A., Hambly, N. C., & Pinfield, D. J. 2004, A&A, 421, 763
Rayner, J. T., Toomey, D. W., Onaka, P. M., et al. 2003, PASP, 115, 362
Reid, I. N., Lewitus, E., Burgasser, A. J., & Cruz, K. L. 2006, ApJ, 639, 1114
Ryan, S. G., Norris, J. E., & Bessell, M. S. 1991, AJ, 102, 303
Schmidt, S. J., West, A. A., Hawley, S. L., & Pineda, J. S. 2010, AJ, 139, 1808
Schneider, A. C., Cushing, M. C., Kirkpatrick, J. D., et al. 2014, AJ, 147, 34
Scholz, R.-D. 2014, A&A, 561, A113
Scholz, R.-D., Bihain, G., Schnurr, O., & Storm, J. 2011, A&A, 532, L5
Scholz, R.-D., Bihain, G., Schnurr, O., & Storm, J. 2012, A&A, 541, A163
Sheppard, S. S., & Cushing, M. C. 2009, AJ, 137, 304
Skrzypek, N., Warren, S. J., Faherty, J. K., et al. 2015, A&A, 574, A78
Stauffer, J., Tanner, A. M., Bryden, G., et al. 2010, PASP, 122, 885
Taylor, B. J. 2005, ApJS, 161, 444
Taylor, M. B. 2006, adass XV, 351, 666
Vacca, W. D., Cushing, M. C., & Rayner, J. T. 2003, PASP, 115, 389
van Leeuwen, F. 2007, A&A, 474, 653